Chronic interleukin-1 drives haematopoietic stem cells towards precocious myeloid differentiation at the expense of self-renewal

Eric M. Pietras[1,6,7], Cristina Mirantes-Barbeito[1], Sarah Fong[1], Dirk Loeffler[2], Larisa V. Kovtonyuk[3], SiYi Zhang[1], Ranjani Lakshminarasimhan[1], Chih Peng Chin[1], José-Marc Techner[1], Britta Will[4], Claus Nerlov[5], Ulrich Steidl[4], Markus G. Manz[3], Timm Schroeder[2], and Emmanuelle Passegué[1,6].

[1] The Eli and Edythe Broad Center for Regenerative Medicine and Stem Cell Research, Department of Medicine, Division of Hematology/Oncology, University of California San Francisco, San Francisco, California, USA.

[2] Department of Biosystems Science and Engineering, ETH Zurich, Basel, Switzerland.

[3] Division of Hematology, University Hospital and University of Zurich, Zurich, Switzerland

[4] Department of Cell Biology, Albert Einstein Medical College, Queens, New York, USA.

[5] Weatherall Institute of Molecular Medicine, Oxford University, Oxford, UK.

[6] Correspondence should be addressed to E.P. (Emmanuelle.Passegue@ucsf.edu) and E.M.P. (eric.pietras@ucdenver.edu)

[7] Present address (E.M.P.): Division of Hematology, University of Colorado Denver, Aurora, Colorado, USA.

Haematopoietic stem cells (HSC) maintain lifelong blood production and increase blood cell numbers in response to chronic and acute injury. However, the mechanism(s) by which inflammatory insults are communicated to HSCs and their consequences for HSC activity remain largely unknown. Here, we demonstrate that interleukin-1 (IL-1), which functions as a key pro-inflammatory 'emergency' signal, directly accelerates cell division and myeloid differentiation of HSCs via precocious activation of a PU.1-dependent gene program. While this effect is essential for rapid myeloid recovery following acute injury to the bone marrow (BM), chronic IL-1 exposure restricts HSC lineage output, severely erodes HSC self-renewal capacity, and primes IL-1-exposed HSCs to fail massive replicative challenges like transplantation. Importantly, these damaging effects are transient and fully reversible upon IL-1 withdrawal. Our results identify a critical regulatory circuit that tailors HSC responses to acute needs, and likely underlies deregulated blood homeostasis in chronic inflammation conditions.

All lineages of haematopoietic cells, including those of the immune system, arise from a rare population of self-renewing HSCs residing in the BM of adult mammals[1]. Blood production by HSCs is regulated by the concerted action of cell-intrinsic transcription factors such as PU.1 and GATA-1, and cell-extrinsic determinants produced by the stromal and haematopoietic components of the BM niche, which together regulate HSC self-renewal and specify lineage commitment[2,3]. While normally maintained in a largely quiescent or dormant state, most HSCs can be rapidly activated to proliferate and differentiate in response to acute needs such as regenerative challenges including myeloablation and transplantation, and physiological insults that induce an inflammatory state[4-6]. Inflammation is a critical physiological process that mediates host defence against invading pathogens, injury and other insults, and is characterized

by rapid mobilization and overproduction of specialized immune cells, particularly myeloid cells[7]. Inflammation is communicated to the haematopoietic system, and HSCs in particular, either by direct sensing via Toll-like receptors (TLRs), or indirectly via a series of pro-inflammatory cytokines[8-10]. In particular, interferons (IFN), both type-I (IFN-α/β) and type-II (IFN-γ), and tumour necrosis factor alpha (TNFα) directly impact HSC fate during an inflammatory response[11-14] and drive HSC specification during embryonic development[15,16]. Pro-inflammatory cytokines are therefore exciting new regulators of HSC function[17], with much remaining to be understood regarding how inflammatory insults tailor blood production under homeostatic and disease conditions.

Interleukin-1 (IL-1) is the first interleukin identified and the founding member of a group of 11 cytokines (IL-1 family), with a central role in responses to infections or sterile insults[18,19]. IL-1 consists of two related genes (*Il1a* and *Il1b*) with distinct regulation but similar biological activities[18], which bind a broadly expressed surface receptor (IL-1R) and trigger downstream transcriptional responses via the adaptor protein MyD88 and a broad range of signalling pathways including NF-κB, p38 MAPK, JNK, and AP-1[20]. IL-1 is a key 'emergency' signal that rapidly activates host defence and repair in many tissues, including the blood system, but also drives tissue dysfunction in the context of chronic inflammation and autoimmune diseases[7,19]. Acute IL-1 signalling is associated with increased myeloid cell production both in culture and *in vivo* in response to infection, irradiation or myeloablative chemotherapy[21-24]. Many of the inflammatory disease conditions associated with chronic IL-1 production such as rheumatoid arthritis (RA), obesity and type-2 diabetes also feature severe haematological complications, including overproduction of tissue-damaging myeloid cells, loss of naïve lymphoid cell production and chronic anemia[25-27]. However, the mechanism by which IL-1 contributes to

deregulated blood output in these conditions, and the functional consequences of both acute and chronic IL-1 exposure on HSC fate, is largely unknown.

RESULTS

IL-1 accelerates HSC differentiation

To investigate IL-1 effects, we isolated HSCs ($Lin^-c\text{-}Kit^+Sca\text{-}1^+Flk2^-CD48^-CD150^+$) (Supplementary Fig. 1a) from wild-type mice and monitored their expansion in liquid culture with or without (±) IL-1α or IL-1β (25 ng/ml). Notably, HSCs cultured with IL-1 differentiated and expanded significantly faster than untreated HSCs over an 8-day period (Fig. 1a), which appeared to result from faster division rates as measured by CFSE dilution assay after 60 hours (Fig. 1b). To confirm accelerated cell division in HSC cultures, we used an automated single-cell tracking approach to continuously monitor cell division over a 6-day period (Fig. 1c)[28]. Remarkably, while the timing of the exit from quiescence first division appeared relatively unaffected in IL-1-treated HSCs, the kinetics of the subsequent differentiation divisions were significantly compressed (Fig. 1d,e). This effect was specific to HSCs, as expansion, survival and proliferation were unchanged in IL-1-treated granulocyte/macrophage progenitors (GMP: $Lin^-c\text{-}Kit^+Sca\text{-}1^-CD34^+Fc\gamma R^+$) and multipotent progenitors (MPP), including myeloid-biased MPP2 ($Lin^-cKit^+Sca1^+Flk2^-CD48^+CD150^+$) and MPP3 ($Lin^-cKit^+Sca1^+Flk2^-CD48^+CD150^-$) or lymphoid-primed MPP4 ($Lin^-cKit^+Sca1^+Flk2^+$)[29,30], which all express IL-1R at similar levels as HSCs (Supplementary Fig. 1a-e). These results indicate that IL-1 specifically targets HSCs and accelerates their division kinetics.

To directly address IL-1 effects on HSC differentiation, we performed colony formation assays in methylcellulose ± IL-1β (Fig. 1f). Strikingly, IL-1-treated HSCs produced almost exclusively myeloid-committed granulocyte/macrophage (GM)-type colonies containing abundant macrophages, in contrast to untreated HSCs, which had a higher proportion of immature multilineage granulocyte/macrophage/megakaryocyte/erythrocyte (GMMkE)-type colonies containing mostly immature myeloblasts and mast cells (Fig. 1g,h). We also re-plated the progeny of these cultures once in methylcellulose without IL-1β, and observed near exhaustion of colony-forming ability in cells from IL-1-treated HSC cultures (Fig. 1i). Moreover, HSCs grown in liquid culture with IL-1β rapidly lost expression of the immaturity markers c-Kit and Sca-1, while gaining expression of the myeloid differentiation markers Mac-1 and FcγR, resulting in greatly increased absolute numbers of c-Kit+ progenitors and mature myeloid cells in IL-1-treated HSC cultures (Fig. 1j,k and Supplementary Fig. 1f). This pro-myeloid differentiation effect was diminished in MPPs and completely absent in GMPs (Supplementary Fig, 2a-e). Collectively, these results demonstrate that IL-1 accelerates the production of mature myeloid cells by HSCs.

Precocious activation of a PU.1 molecular circuit

To understand IL-1 effects at the molecular level, we used qRT-PCR and a custom-made Fluidigm PCR array to analyse gene expression in HSCs cultured ± IL-1β for 12 or 24 hours (Fig. 2a and Supplementary Fig. 3a). Remarkably, we observed a strong induction of the transcription factor PU.1 (*Spi1*) and its target genes GM-CSFR (*Csf2ra*) and M-CSFR (*Csf1r*) in IL-1-treated HSCs (Fig. 2b and Supplementary Fig. 3b). In contrast, lymphoid and megakaryocyte/erythrocyte (MkE) lineage genes were largely unaffected, suggesting that IL-1

functions by activating, rather than suppressing, lineage-specific gene programs in HSCs[31]. Consistent with the effects of IL-1 on cell division, we also observed activation of the cell cycle machinery and decreased expression of the quiescence-enforcing cyclin D1 (*Ccnd1*) and p57 (*Cdkn1c*) genes, alongside induction of p21 (*Cdkn1a*), another PU.1 target (Fig. 2b). We confirmed rapid upregulation of M-CSFR and two other PU.1-dependent myeloid surface markers, Mac-1 and CD18, in IL-1-treated HSCs (Fig. 2c), and found limited or absent activation of PU.1 and its target genes in IL-1-treated MPPs and GMPs (Supplementary Fig. 3b) Moreover, using HSCs isolated from *PU.1-eYFP* reporter mice, we confirmed fast upregulation of PU.1 activity upon IL-1 exposure, with uniformly high PU.1 levels in IL-1-treated *PU.1-eYFP* HSCs prior to their first division in single-cell tracking experiments (Fig. 2d,e, and Supplementary Fig. 3c). We also uncovered a small subpopulation of PU.1^{hi} HSCs in untreated cultures whose progeny showed division kinetics similar to IL-1-treated HSCs (Supplementary Fig. 3d). In particular, both had a delayed first division when compared to untreated PU.1^{lo} HSCs, consistent with the decreased BrdU incorporation observed after 24 hours in IL-1-treated HSCs (Supplementary Fig. 3e). The subsequent divisions of untreated PU.1^{hi} HSCs were also accelerated, thus directly linking elevated PU.1 activity with the overall effect of IL-1 in accelerating division kinetics. This is in contrast to the recently reported function of steady-state PU.1 levels in limiting HSC cell cycle re-entry[32] and likely reflects differences in gene dosage. In fact, high PU.1 levels similarly delayed HSC first division while simultaneously priming their progeny to undergo accelerated proliferation via induction of myeloid lineage determinants and cell cycle activators including *Cdk4*, *Myc*, *Ccnb* and *Ccne1* (Fig. 2b). To directly demonstrate the importance of PU.1 for IL-1 effects, we isolated HSCs from *PU.1*$^{\Delta URE}$ hypomorphic mice lacking the *PU.1* upstream regulatory element (URE) and expressing PU.1 at 10-20% normal

levels[33]. Strikingly, myeloid differentiation, including Mac-1 expression, was severely attenuated in *PU.1*$^{\Delta URE}$ HSC cultures (Fig. 2f), confirming the requirement for PU.1 in IL-1-driven HSC differentiation. Moreover, to establish that PU.1 upregulation is sufficient to drive accelerated HSC differentiation, we overexpressed PU.1 in HSC using a validated lentiviral vector[34]. Similar to IL-1-treated HSCs, PU.1-overexpressing HSCs showed accelerated gain of the myeloid markers Mac-1/FcγR relative to control HSCs (Fig. 2g). These results establish that IL-1 acts instructively and 'primes' HSCs to undergo accelerated myeloid differentiation via precocious activation of a PU.1-dependent molecular circuit.

Mechanism of PU.1 activation

To gain insight into the mechanism of PU.1 activation by IL-1, we first addressed its dependency on IL-1R signalling. As expected, *Il1r1*$^{-/-}$ HSCs did not show accelerated myeloid differentiation in the presence of IL-1β (Fig. 3a), and IL-1-treated *Il1r1*$^{-/-}$*::PU.1-eYFP* HSCs failed to upregulate PU.1 (Fig. 3b). We then exposed *PU.1-eYFP* HSCs cultured for 12 hours ± IL-1β (25 pg/ml, a lower dose titrated for sensitivity), to inhibitors of various signalling pathways acting downstream of IL-1R (Fig. 3c,d and Supplementary Fig. 3f,g)[20]. Interestingly, while blockade of p38, MEK and PKC partially decreased IL-1-induced PU.1 levels, inactivation of IKK almost entirely abolished PU.1 activity, consistent with the ability of its downstream target, NF-κB, to bind the PU.1 promoter[35]. On the other hand, PI3K and mTOR inhibition had no effect, while blockade of Src kinase, which drives PU.1 activation downstream of M-CSFR[36], only partially inhibited IL-1 effects. Since M-CSFR expression was increased in IL-1-treated HSCs, we also tested whether IL-1 could directly activate an M-CSF autocrine loop to induce PU.1. However, treatment with an anti-M-CSFR blocking antibody did not attenuate IL-1-

mediated PU.1 activation in *PU.1-eYFP* HSCs, despite preventing M-CSF-mediated macrophage differentiation in BM cultures (Fig. 3e, Supplementary Fig. 3h). Furthermore, the effect of IL-1 required constant IL-1R signalling and was lost if IL-1 was washed out after 24 hours (Fig. 3f), further arguing against a role for IL-1-induced secondary factors. These results demonstrate that direct and sustained IL-1 signalling, mediated largely through NF-κB pathway activation downstream of IL-1R, is required for PU.1 induction.

Haematopoietic remodelling following IL-1 exposure

To investigate IL-1 effects on haematopoiesis *in vivo*, we injected mice intraperitoneally with 0.5 μg IL-1β for 1 day (acute treatment) up to 20 consecutive days (chronic exposure) (Fig. 4a). As expected, IL-1-treated mice exhibited a rapid and sustained increase in circulating myeloid cells, with concomitant decreases in lymphoid cells and erythrocytes (Fig. 4b,c and Supplementary Fig. 4a). In the BM, 1 day acute IL-1 treatment did not significantly alter the overall cellularity or mature cell populations, save for a small but significant increase in $Mac1^{+}Gr1^{int}$ pre-granulocytes/monocytes (preGr) (Supplementary Fig. 4b-d). However, acute IL-1 treatment already resulted in a rapid MPP expansion and substantial erosion of common lymphoid progenitors (CLP: $Lin^{-}Flk2^{+}IL\text{-}7R^{+}c\text{-}Kit^{int}Sca\text{-}1^{int}$) (Supplementary Fig. 4c,d), suggesting quick myeloid priming upon IL-1 exposure. These changes were maintained and associated with a clear rebalancing of lineage output upon 20 days chronic IL-1 exposure, with significant expansion of $Mac\text{-}1^{+}Gr\text{-}1^{+}$ granulocytes (Gr) and corresponding loss of $B220^{+}CD19^{+}$ B cells (Fig. 4d). This was associated with a specific amplification of GMPs and myeloid-biased MPP2 and MPP3 subsets (Fig. 4e), suggesting direct activation of a myeloid differentiation axis at the level of HSCs[28]. Consistently, we observed a rapid and sustained increase in the

metabolically activated MPP1 ($Lin^-cKit^+Sca1^+Flk2^-CD48^-CD150^+CD34^+$), which is produced by dormant long-term HSCs (HSC^{LT}; $Lin^-cKit^+Sca1^+Flk2^-CD48^-CD150^+CD34^-$)[29], and solely accounted for the overall expansion of phenotypic HSCs observed upon 20 days chronic IL-1 exposure (Fig. 4g and Supplementary Fig. 4e). Importantly, HSC activation and BM remodelling was not observed in IL-1-treated *Il1r1*$^{-/-}$ mice, confirming its dependency on IL-1R signalling (Supplementary Fig. 4e). Moreover, using a sensitive *in vivo* CFSE dilution assay[37] and 7 consecutive days of IL-1β treatment, we demonstrated that fewer IL-1-treated HSC^{LT} remain in an undivided state compared to untreated HSC^{LT} (Fig. 4h,i and Supplementary Fig. 5a,b). This confirms *in vivo* that IL-1 exposure directly increases HSC division rates, which likely fuels the MPP overproduction observed even after acute treatment. In addition, we showed persistent PU.1 activation in a substantial fraction of HSCs from *PU.1-eYFP* mice upon both acute and chronic IL-1 treatment (Fig. 4j). We also found decreased *Cebpa* levels and increased *Runx1* expression in HSCs exposed to IL-1 for 20 days (Fig. 4k), which is strikingly similar to the molecular changes observed in regenerating HSCs that overproduce myeloid-biased MPP2/3 as they re-build the myeloid lineage[30]. PU.1 was also activated in MPP4 from IL-1-treated *PU.1-eYFP* mice (Supplementary Fig. 5c), which likely reflects the myeloid lineage reprogramming of this lymphoid-primed MPP subset upon IL-1 exposure. This is consistent with the observed loss of lymphoid output and previously reported inhibition of lymphopoiesis by IL-1[38]. Collectively, these results indicate that *in vivo* IL-1 exposure triggers a rapid PU.1-mediated myeloid differentiation program in HSCs, which amplifies myeloid cell production at the expense of the other blood lineages.

Acute IL-1 stimulation contributes to myeloid recovery

196 To interrogate the importance of IL-1 for blood regeneration, we focused on 5-
197 fluorouracil (5-FU)-mediated myeloablation, as we found that both IL-1α and IL-1β levels were
198 significantly increased in BM plasma, but not in blood serum, while no other pro-inflammatory
199 cytokines were induced following one injection of 150 mg/kg 5-FU (Fig. 5a and Supplementary
200 Fig. 6a). To identify the cellular source(s) of IL-1, we analysed *Il1a* and *Il1b* expression by qRT-
201 PCR in mature BM myeloid and lymphoid cells, as well as in BM stromal populations[39],
202 specifically osteoblastic lineage cells (OBC: $Lin^-CD45^-Sca\text{-}1^-CD51^+$), multipotent stromal cells
203 (MSC: $Lin^-CD45^-Sca\text{-}1^+CD51^+$) and endothelial cells (EC: $Lin^-CD45^-Sca\text{-}1^+CD31^+$)
204 (Supplementary Fig. 6b). At steady state, *Il1a* was expressed largely by BM $CD4^+$ T cells, and
205 *Il1b* by Grs (Fig. 5b). However, upon 5-FU treatment, *Il1a* was strongly induced in myeloid cells
206 and ECs, while no increase in *Il1b* expression was detected, suggesting that it might be released
207 by dying Grs upon inflammasome activation[40]. Strikingly, myeloid recovery was significantly
208 and specifically delayed in 5-FU-injected $Il1r1^{-/-}$ mice (Fig. 5c), emphasizing the importance of
209 IL-1R signalling for myeloid recovery following BM injury. However, HSCs isolated from
210 $Il1r1^{+/+}$ and $Il1r1^{-/-}$ mice 10 days post-5-FU treatment, and at the peak of IL-1 production,
211 displayed equivalent engraftment and long-term multilineage reconstitution upon transplantation
212 (Fig. 5d-g). This indicates that acute exposure to IL-1 and transient activation of pro-myeloid
213 differentiation pathways required for optimal blood recovery does not affect HSC self-renewal
214 activity. In addition, $Il1r1^{-/-}$ mice had unaffected blood production as previously described[41], and
215 normal stem and progenitor BM compartments, aside from a specific decrease in myeloid-biased
216 MPP3 that may represent impaired basal myeloid lineage priming in the absence of tonic IL-1
217 signalling (Supplementary Fig. 6c,d). Together, these results demonstrate that while IL-1
218 signalling is dispensable in HSCs at steady state, it becomes important in physiological

'emergency' conditions when acute IL-1 production rapidly activates HSC myeloid differentiation to enhance blood regeneration. They also identify ECs as one of the key producers of IL-1 following haematopoietic damage, consistent with a local delivery of IL-1 to quiescent HSCs lodged in their perivascular BM niches[42].

Chronic IL-1 exposure impairs HSC function

To better understand the consequence of chronic IL-1 exposure, we used HSCs isolated from mice injected ± IL-1β for 20 days. First, we confirmed that IL-1-treated HSCs had unaffected clonogenic efficiency in methylcellulose and normal survival as measured by cleaved caspase-3 (CC3) levels compared to naïve HSCs isolated from PBS-treated mice (Supplementary Fig. 7a). We then transplanted both naïve and IL-1-treated HSCs into sub-lethally irradiated congenic recipients that were subsequently injected ± IL-1β for another 30 days to track lineage reconstitution and BM HSC chimerism (Fig. 6a). We observed accelerated donor blood output from naïve HSCs exposed to IL-1 after transplantation (Fig. 6b), which is consistent with earlier literature describing enhanced myeloid regeneration in similar conditions[21]. In contrast, donor blood output rapidly eroded in mice transplanted with IL-1-treated HSCs upon continued IL-1 exposure (Fig. 6b and Supplementary Fig. 7b). In both cases, IL-1 treatment following transplantation completely blocked donor lymphoid output and rebalanced blood production towards enhanced myelopoiesis (Fig. 6c and Supplementary Fig. 7b). However, chimerism analyses uncovered a near complete exhaustion of donor HSCs in the BM of mice transplanted with IL-1-treated HSCs, even in recipients not subsequently injected with IL-1 (Fig. 6d and Supplementary Fig. 7c). To determine whether these effects were due to IL-1-mediated PU.1 activation, we transplanted lentivirus-transduced HSCs overexpressing PU.1 into sub-lethally

irradiated recipient mice and tracked these mice for 30 days (Fig. 6e). Strikingly, compared to control-transduced HSCs, we observed rapid erosion of donor blood output and complete exhaustion of PU.1-overexpressing HSCs in the BM (Fig. 6f,g and Supplemental Fig. 7d), a behaviour similar to IL-1-exposed HSCs. Together, these short-term lineage-tracking results indicate that while IL-1 treatment always enhances myeloid cell production regardless of its duration, it also severely compromises HSC function and blood regeneration in conditions of chronic exposure, likely via hyperactivation of PU.1.

To confirm the functional impairment of HSCs chronically exposed to IL-1, we transplanted naïve and IL-1-treated HSCs into lethally irradiated recipient mice to assess long-term engraftment and self-renewal activity after 4 months, and also performed limiting dilution analyses (LDA) with unfractionated BM cells to address HSC function independently of surface markers (Fig. 7a and Supplemental Fig. 8a). In both cases, we observed significantly decreased donor chimerism and reduced lymphoid output from IL-1-treated HSCs (Fig. 7b,c and Supplementary Fig. 8b,c), reflecting compromised self-renewal activity. To investigate whether long-term IL-1 treatment could lead to HSC exhaustion, we also injected mice ± IL-1β for a total of 70 days (Fig. 7d). Remarkably, even after such a long exposure, the HSC pool remained numerically intact though with an elevated frequency and number of myeloid-primed $CD41^{+}$ HSC^{LT} [43-45] and expansion of myeloid-biased MPP2/3 (Supplementary 8d,e). We also found that 70 day IL-1-treated HSC^{LT} had unaffected survival in methylcellulose (Supplementary Fig. 8f), but significantly impaired self-renewal activity following transplantation (Fig. 7,e,f). These results demonstrate that chronic IL-1 exposure restricts HSC lineage output and severely compromises HSC regenerative function, thus priming IL-1-exposed HSCs to fail replicative challenges like transplantation.

IL-1 effects are reversible upon withdrawal

Lastly, we tested whether the damaging effects of chronic IL-1 exposure were retained by the HSC pool. We first re-transplanted into lethally irradiated recipient mice donor HSCs harvested from mice initially reconstituted with naïve and IL-1-exposed HSCs (20 days or 70 days) (Fig. 7g and Supplementary Fig. 8g). Remarkably we observed a complete recovery relative to naïve controls in donor chimerism and lineage output in HSCs derived from IL-1-treated donor mice, regardless of the length of the original IL-1 exposure (Fig. 7h,i and Supplementary Fig. 8h,i). These results suggest that the remaining portion of the IL-1-exposed HSC pool was not functionally compromised. To assess whether IL-1 effects were reversible under native conditions, we used mice that were injected ± IL-1β for 20 days and allowed to rest without further treatment for 8 weeks (Fig. 8a). After the rest period, blood parameters had fully normalized to untreated levels with a complete restoration of myeloid and B cell numbers (Fig. 8b). Moreover, most of the BM changes had also reverted to untreated levels, with normal numbers of HSCs and MPPs, including MPP1, and restoration of the CLP compartment (Fig. 8c,d). The only persisting differences were increased GMP and decreased MPP4 numbers, likely reflecting residual myeloid priming effects of the initial IL-1 treatment. Most importantly, donor chimerism and lymphoid output were indistinguishable from untreated HSCs, indicating full restoration of self-renewal activity (Fig. 8e,f). Taken together, these results demonstrate that the damaging effects of chronic IL-1 exposure on HSC regenerative functions are fully reversible upon interruption of IL-1 exposure.

DISCUSSION

Our results demonstrate that IL-1 directly regulates HSC fate and instructs quick myeloid differentiation via precocious activation of an instructive PU.1 gene program and exclusive production of myeloid cells in 'emergency' situations such as myeloablation and transplantation (Fig. 8g)[46]. These results imply that previous models, in which sustained low PU.1 levels initiate eventual myeloid commitment in progenitors[47], do not apply in stress conditions. IL-1 has long been known to inhibit lymphopoiesis and erythopoiesis[38,48,49] though, paradoxically, high PU.1 levels also play a key role in B cell development[47]. It is therefore likely that rapid PU.1 induction in HSCs by IL-1 drives myelopoiesis while preventing the establishment of other gene programs specifying lymphopoiesis and erythropoiesis. Interestingly, PU.1 activation proceeds via IKK kinase, which is the primary activator of NF-κB, a known IL-1 target that is also downstream of TLRs[20]. As TLRs also induce HSC myeloid differentiation[50], it is possible that PU.1 serves as a convergence point for these pro-inflammatory signals. Interestingly, the transcription factor C/EBPβ also regulates 'emergency' myeloid differentiation in response to IL-3 or GM-CSF in haematopoietic progenitors[51], or to IFN-γ stimulation in HSCs[52]. It will therefore be interesting to investigate whether activation of PU.1 and C/EBPβ represents distinct or converging mechanisms accelerating HSC myeloid differentiation in response to inflammation.

Our results also demonstrate that chronic IL-1 exposure significantly impairs HSC function. Notably, the numerical HSC pool is not depleted, consistent with prior results of long-term *in vivo* exposure to IFN-α[13]. This may reflect the recently described ability of the MPP compartment to 'buffer' myeloid demand independently of HSCs[53,54], or the replenishment of an IL-1-responsive HSC subset from quiescent HSC^{LT} similar to the IFN-responsive $CD41^{+}$ HSCs recently involved in emergency megakaryopoiesis[55]. This latest interpretation is supported by our observation that a fraction, rather than all, HSCs activate PU.1 following IL-1 exposure, and the

partial, rather than complete, functional impairment of IL-1-exposed HSCs. In this context, neither CD34 nor CD41 expression appears to separate IL-1 responsive from IL-1 non-responsive HSC^{LT}, and further analyses will be required to identify ways to separate these two functional subsets. Interestingly, the deleterious effects of chronic IL-1 exposure on HSC function are largely resolved following IL-1 withdrawal, suggesting they are not permanently 'imprinted' onto the HSC pool via epigenetic or other means. As IL-1 receptor blockers including Anakinra are highly efficacious treatments for a wide range of chronic inflammatory diseases featuring deregulated blood production[19], restoration of HSC function could be a key benefit of IL-1 blockade. Moreover, it is likely that IL-1 could plays a similar dual role, both beneficial and pathogenic, in a variety of tissues by directly reprogramming their stem cell populations. Collectively, our findings demonstrate that IL-1 acts as a double-edged sword for HSC function, promoting myeloid regeneration without functional cost to HSCs during acute need, but significantly impairing their self-renewal and lineage output following chronic exposure. Modulation of IL-1 signalling, particularly its duration, may therefore be an important approach for broadly improving stem cell health and tissue function in the context of chronic inflammation or physiological aging.

ACKNOWLEDGEMENTS

We thank M. Kissner and M. Lee for management of our Flow Cytometry Core Facility and members of the Passegué laboratory for insights and suggestions. E.M.P. was supported by NIH F32 HL106989 and K01 DK09831, C.M-B. by an Institute of Health Carlos III (ISCIII) fellowship, R.L by a CIRM Bridges internship and M.G.M. by the Swiss National Science Foundation (310030_146528/1). E.P. and research were supported by a LLS Scholar Award and NIH R01 HL092471. The authors have no financial interests to disclose.

AUTHOR CONTRIBUTIONS

E.M.P performed all the experiments with assistance from C.M-B. and S.F. D.L. helped with the single-cell continuous tracking experiments that were performed in T.S. laboratory. R.L. helped with the *Il1r1*$^{-/-}$ and 5-FU analyses, J-M.T. with the *in vitro* cultures, C.P.C with analysis of single-cell tracking experiments, L.K. and M.G.M. with the *in vivo* CFSE dilution experiments, B.W. and U.S. with the *PU.1*$^{\Delta URE}$ experiments, and C.N. provided *PU.1-EYFP* reporter mice. E.M.P, C.M., S.F. and E.P. designed the experiments and interpreted the results. E.M.P. and E.P. wrote the manuscript.

COMPETING FINANCIAL INTERESTS

The authors declare no competing financial interests.

REFERENCES

1. Orkin, S.H. & Zon, L.I. Hematopoiesis: an evolving paradigm for stem cell biology. *Cell* **132**, 631-644 (2008).

2. Iwasaki, H. & Akashi, K. Myeloid lineage commitment from the hematopoietic stem cell. *Immunity* **26**, 726-740 (2007).

3. Schepers, K., Campbell, T.C. & Passegué, E. Normal and leukemic stem cell niches: insights and therapeutic opportunities. *Cell Stem Cell* **16**, 254-267 (2015).

4. Wilson, A. *et al*. Hematopoietic stem cells reversibly switch from dormancy to self-renewal during homeostasis and repair. *Cell* **135**, 1118-1129 (2008).

5. Pietras, E.M., Warr, M.R., & Passegué, E. Cell cycle regulation in hematopoietic stem cells. *J Cell Biol* **195**, 709-720 (2011).

6. Takizawa, H., Boettcher, S. & Manz, M.G. Demand-adapted regulation of early hematopoiesis in infection and inflammation. *Blood* **119**, 2991-3002 (2012).

7. Medzhitov, R. Origin and physiological roles of inflammation. *Nature* **454**, 428-435 (2008).

8. Nagai, Y. *et al*. Toll-like receptors on hematopoietic progenitor cells stimulate innate immune system replenishment. *Immunity* **24**, 801-812 (2006).

9. Scheuttpelz, L.G. & Link, D.C. Regulation of hematopoietic stem cell activity by inflammation. *Front Immunol* **4** doi: 10.3389/fimmu.2013.00204 (2013).

10. Mirantes, C., Passegué, E. & Pietras, E.M. Pro-inflammatory cytokines: emerging players regulating HSC function in normal and diseased hematopoiesis. *Exp Cell Res* **329**, 248-254 (2014).

11. Essers, M., *et al*. IFNalpha activates dormant haematopoietic stem cells in vivo. *Nature* **458**, 904-908 (2009).

12. Baldridge, M.T., King, K.Y., Boles, N.C., Weksberg, D.C., & Goodell, M.A. Quiescent haematopoietic stem cells are activated by IFN-gamma in response to chronic infection. *Nature* **465**, 793-797 (2010).

13. Pietras, E.M. *et al*. Re-entry into quiescence protects hematopoietic stem cells from the killing effect of chronic exposure to type I interferons. *J Exp Med* **211**, 245-262 (2014).

14. Pronk C.J., Veiby, O.P., Bryder, D., & Jacobsen, S.E. Tumor necrosis factor restricts hematopoietic stem cell activity in mice: involvement of two distinct receptors. *J Exp Med* **208**, 1563-1570 (2011).

15. Espín-Palazón, R *et al*. Proinflammatory signaling regulates hematopoietic stem cell emergence. *Cell* **159**, 1070-1085 (2014).

16. Li, Y *et al*. Inflammatory signaling regulates embryonic hematopoietic stem and progenitor cell production. *Genes Dev* **28,** 2597-2612 (2014).

17. King, K.Y., & Goodell, M.A. Inflammatory modulation of HSCs: viewing the HSC as a foundation for the immune response. *Nat Rev Immunol* **11**, 685-692 (2011).

18. Sims, J.E. & Smith, D.E. The IL-1 family: regulators of immunity. *Nat Rev Immunol* **10**,

382 89-102 (2010).

383 19. Dinarello, C.A., Simon, A. & van der Meer, J.W. Treating inflammation by blocking
384 interleukin-1 in a broad spectrum of diseases. *Nat Rev Drug Discov* **11**, 633-652 (2012).

385 20. Martin, M.U. & Wesche, H. Summary and comparison of the signaling mechanisms of
386 the Toll/interleukin-1 receptor family. *BBA Mol Cell Res* **1592**, 265-280 (2002).

387 21. Morrissey, P., Charrier, K., Bressler, L. & Alpert, A. The influence of IL-1 treatment on
388 the reconstitution of the hemopoietic and immune systems after sublethal irradiation. *J*
389 *Immunol* **140**, 4204-4210 (1988).

390 22. Damia, G. et al. Prevention of acute chemotherapy-induced death in mice by recombinant
391 human interleukin 1: protection from hematological and nonhematological toxicities.
392 *Cancer Res* **52**, 4082-4089 (1992).

393 23. Hestdal, K. et al. Interleukin-1 (IL-1) directly and indirectly promotes hematopoietic cell
394 growth through type I IL-1 receptor. *Blood* **84**, 125-132 (1994).

395 24. Ueda, Y., Cain, D.W., Kuraoka, M., Kondo, M. & Kelsoe, G. IL-1R type I-dependent
396 hematopoietic stem cell proliferation is necessary for inflammatory granulopoieisis and
397 reactive neutrophilia. *J Immunol* **182**, 6477-6484 (2009).

398 25. Smith, M.A., Knight, S.M., Maddison, P.J. & Smith, J.G. Mechanism of anaemia in
399 rheumatoid arthritis: effect of the blunted response to erythropoietin and of interleukin 1
400 production by marrow macrophages. *Ann Rheum Dis* **51**, 753-757 (1992).

401 26. Dinarello, C.A. Blocking IL-1 in systemic inflammation. *J Exp Med* **201**, 1355-1359

(2005).

27. Cain, D., Kondo, M., Chen, H. & Kelsoe, G. Effects of acute and chronic inflammation on B-cell development and differentiation. *J Invest Dermatol* **129**, 266-277 (2009).

28. Rieger, M.A., Hoppe, P.S., Smejkal, B.M., Eitelhuber, A.C. & Schroeder, T. Hematopoietic cytokines can instruct lineage choice. *Science.* **325**, 217-218 (2009).

29. Cabezas-Wallscheid, N. *et al*. Identification of regulatory networks in HSCs and their immediate progeny via integrated proteome, transcriptome, and DNA methylome analysis. *Cell Stem Cell* **15**, 507-22 (2014).

30. Pietras, E.M *et al*. Functionally distinct subsets of lineage-biased multipotent progenitors control blood production in normal and regenerative conditions. *Cell Stem Cell* **17**, 35-46 (2015).

31. Enver, T. & May, G. Lineage Specification: Reading the Instructions May Help! *Current Biology* **23**, R662-R665 (2013).

32. Staber, P.B. *et al*. Sustained PU.1 levels balance cell-cycle regulators to prevent exhaustion of adult hematopoietic stem cells. *Mol Cell* **49**, 934-946 (2013).

33. Rosenbauer, F. *et al*. Acute myeloid leukemia induced by graded reduction of a lineage-specific transcription factor, PU.1. *Nat Genet* **36**, 624-630 (2013).

34. Steidl, U., *et al*. A distal single nucleotide polymorphism alters long-range regulation of the PU.1 gene in acute myeloid leukemia. *J Clin Invest* **117**, 2611-2620 (2007).

35. Bonadies, N. *et al*. PU.1 is regulated by NF-kappaB through a novel binding site in a

17kb upstream enhancer element. *Oncogene* **18**, 1062-1072 (2010).

36. Mossadegh-Keller, N. *et al*. M-CSF instructs myeloid lineage fate in single haematopoietic stem cells. *Nature* **497**, 239-243 (2013).

37. Takizawa, H., Regoes, R.R., Boddupalli, C.S., Bonhoeffer, S. & Manz, M.G. Dynamic variation in cycling of hematopoietic stem cells in steady state and inflammation. *J Exp Med* **208**, 273-284 (2011).

38. Dorshkind, K. IL-1 inhibits B cell differentiation in long term bone marrow cultures. *J Immunol* **6**, 1191-1197 (1988).

39. Schepers, K. *et al*. Myeloproliferative neoplasia remodels the endosteal bone marrow niche into a self-reinforcing leukemic niche. *Cell Stem Cell* **13**, 285-299 (2013).

40. Cullen, S.P., Kearney, C.J., Clancy, D.M., and Martin, S.J. Diverse activators of the NLRP3 inflammasome promote IL-1β secretion by triggering necrosis. *Cell Reports* **11**, 1535-1548 (2015).

41. Glaccum, M.B. *et al*. Phenotypic and functional characterization of mice that lack the type I receptor for IL-1. *J Immunol* **159**, 3364-3371 (1997).

42. Mendelson, A. & Frenette, P.S. Hematopoietic stem cell niche maintenance during homeostasis and regeneration. *Nat Med* **20**, 833-846 (2014).

43. Gekas, C. & Graf, T. CD41 expression marks myeloid-biased adult hematopoietic stem cells and increases with age. *Blood* **121**, 4463-4472 (2013).

44. Yamamoto, R., *et al*. Clonal analysis unveils self-renewing lineage-restricted progenitors

generated directly from hematopoietic stem cells. *Cell* **154**, 1112-1126 (2013).

45. Miyawaki, K., *et al*. CD41 marks the initial myelo-erythroid specification in adult mouse hematopoiesis: redefinition of murine common myeloid progenitor. *Stem Cells* **33**, 976-987 (2015).

46. Manz, M.G. & Boettcher, S. Emergency granulopoiesis. *Nat Rev Immunol* **14**, 302-314 (2014).

47. Dakic, A., Wu, L. & Nutt, S.A. Is PU.1 a dosage-sensitive regulator of haemopoietic lineage commitment and leukaemogenesis? *Trends Immunol* **28**, 108-114 (2007).

48. Adamson, J.W. The anemia of inflammation/malignancy: mechanisms and management. *Hematology Am Soc Hematol Educ Program* 159-165. doi: 10.1182/asheducation-2008.1.159 (2008).

49. Zhang, P *et al*. PU.1 inhibits GATA-1 function and erythroid differentiation by blocking GATA-1 DNA binding. *Blood* **96**, 2641-2648 (2000).

50. Zhao, J.L. *et al*. Conversion of danger signals into cytokine signals by hematopoietic stem and progenitor cells for regulation of stress-induced hematopoieisis. *Cell Stem Cell* **14**, 445-459 (2014).

51. Hirai, H. *et al*. C/EBPβ is required for 'emergency'granulopoiesis. *Nat Immunol* **7**, 732-739 (2006).

52. Matatall, K.A., Shen, C.C., Challen, G.A., & King, K.Y. Type II interferon promotes differentiation of myeloid-biased hematopoietic stem cells. *Stem Cells* **32**, 3023-3030

(2014).

53. Sun, J. *et al*. Clonal dynamics of native haematopoiesis. *Nature* **514**, 322-327 (2014).

54. Busch, K. *et al*. Fundamental properties of unperturbed haematopoiesis from stem cells in vivo. *Nature* **518**, 542-546 (2015).

55. Haas, S. *et al*. Inflammation-induced emergency megakaryopoiesis driven by hematopoietic stem cell-like megakaryocyte progenitors. *Cell Stem Cell* **17**, 422-434 (2015).

FIGURE LEGENDS

Figure 1 | IL-1 accelerates HSC differentiation along the myeloid lineage. a, Representative expansion in liquid culture (n = 3 biological replicates/group). **b**, CFSE dilution assays after 60 hours. Data represent one of 2 replicate experiments. Grey histogram shows −IL-1β HSCs at 24 hours. **c-e** Continuous single-cell tracking experiments (n = 47 and 51 HSC/group): (**c**) experimental design, (**d**) single-cell pedigrees of median division times, and (**e**) box plot quantification of division times. Results show median (lines) and 10-90th percentile (whiskers). **f-i**, Colony forming unit (CFU) assays in methylcellulose: (**f**) experimental design, (**g**) single cell clonogenic assays (n = 3 replicate experiments with 60 HSC/group), (**h**) representative colony type (scale bar, 100 μm) and morphology (scale bar, 10 μm; arrow indicates a macrophage), and (**i**) replating (repl.) experiments. Data represent one of two replicate experiments. Colonies were scored after 7 days. MkE: megakaryocyte/erythrocyte; M: macrophage; G: granulocyte; GM: ganulocyte/macrophage; GMMkE: mix colony. **j-k**, Myeloid differentiation in liquid culture (n = 6 biological replicates/group): (**j**) experimental design with representative FACS plots, and (**k**) quantification of myeloid marker expression. Source data for **a** are shown in Supplementary Table 1. Data are means ± S.D.; * $p \leq 0.05$, ** $p \leq 0.01$, *** $p \leq 0.001$. *P*-values in **a** were determined by one-way ANOVA with Dunnet's test, in **g** by paired Student's *t* test, and in **e** and **k** by Mann-Whitney *u* test. Exact *P*-values number of replicates used to derive statistical data (n) and statistical tests used are shown in Supplementary Table 2.

Figure 2 | IL-1 induces precocious activation of a PU.1 gene program in HSCs. a-b, Fluidigm gene expression analyses of lineage determinant and cell cycle genes: (**a**) heatmap, and (**b**) expression of individual genes (n = 8 pools of 100 cells for each condition; bars: means).

Results are expressed as fold changes compared to levels in -IL-1β HSCs (set to 1). My: myeloid; Ly: lymphoid; MkE: megakaryocyte/erythroid. (**c**) Expression of PU.1 targets (n = 5 biological replicates/group; M-CSFR day 4, n = 7). (**d**) Representative histogram and PU.1 levels in *PU.1-eYFP* HSCs (n = 6 biological replicates/group; day 8, n = 4). Results are expressed as mean fluorescence intensity (MFI) levels. (**e**) Representative images and PU.1 levels in individual *PU.1-eYFP* HSCs prior to first division (n = 33-37 HSC/group; scale bar, 10 μm). Results are expressed in arbitrary units (AU) and box plots show median (lines) with 10-90th percentile (whiskers). (**f**) Experimental design and myeloid marker expression in control (Ctrl) and *PU.1*$^{\Delta URE}$ (ΔURE) HSCs (n = 3 biological replicates/group). (**g**) Experimental design, representative FACS plots and myeloid marker expression in lentivirally transduced (GFP^{+}) Ctrl or PU.1-overexpressing HSCs (n = 3 biological replicates/group for day 4; day 1 represents the mean of two biological replicates/group). Source data for **d**, **f** and **g** are shown in Supplementary Table 1. Data are means ± S.D.; * $p \leq 0.05$, ** $p \leq 0.01$, *** $p \leq 0.001$. *P*-values in **b-e** were determined by Mann-Whitney *u* test, in **f** by one-way ANOVA with Dunnet's test, and in **g** by paired Student's *t* test. Exact *P*-values, number of replicates used to derive statistical data (n),and statistical tests used are shown in Supplementary Table 2.

Figure 3 | PU.1 activation requires direct and sustained IL-1R signalling. (**a**) Experimental design and myeloid marker expression in *Il1r1*$^{-/-}$ HSCs (n = 3 biological replicates/group). (**b**) Experimental design and PU.1 levels in *Il1r1*$^{+/+}$ and *Il1r1*$^{-/-}$*::PU.1-eYFP* HSCs (n = 3 biological replicates/group). (**c**) Experimental design, representative histograms, and PU.1 levels in *PU.1-eYFP* HSCs treated with the indicated inhibitors (n = 3 biological replicates/group for MEK, Src, PI3K; n = 4 for p38, PKC, mTOR; n = 7 for IKK). Data are expressed as $\log_2$ fold change in

PU.1-eYFP MFI levels relative to -IL-1β *PU.1-eYFP* HSCs. (**d**) Schematic of the signalling pathways downstream of IL-1R highlighting NF-κB and indicating the connection with M-CSFR signalling. (**e**) Experimental design, representative histograms and PU.1 levels in *PU.1-eYFP* HSCs treated with anti-M-CSFR blocking antibody (aMR) or isotype control (iso) (n = 3 biological replicates/group). (**f**) Experimental design, representative FACS plots and myeloid marker expression in IL-1 wash out (wo) experiments (n = 3 biological replicates/group). Source data for **a-c**, **e** and **f** are shown in Supplementary Table 1. Data are means ± S.D.; * $p \leq 0.05$, ** $p \leq 0.01$, *** $p \leq 0.001$. *P*-values in **a** were determined by Mann-Whitney *u* test, in **b** and **e** by paired Student's *t* test, and in **c** and **f** by one way ANOVA with Tukey's and Dunnet's tests, respectively. Exact *P*-values, number of replicates used to derive statistical data (n), and statistical tests used are shown in Supplementary Table 2

Figure 4 | IL-1 enforces HSC myeloid differentiation *in vivo*. a-c Peripheral blood (PB) parameters in mice injected ±IL-1β for 20 days: (**a**) experimental design, (**b**) percentage of myeloid (Mac-1$^+$Gr-1$^+$) and lymphoid (B220$^+$ and CD3$^+$) cells over time (n = 5 mice/group; * *vs.* -IL-1β; ° *vs.* day 0), and (**c**) complete blood counts after 20 days. My: myeloid; Ly: lymphoid; RBC: red blood cell; Plt: platelet. **d-g** Size of the indicated BM populations in mice injected ± IL-1β for 20 days (n = 18 mice/group) **h-i** *In vivo* CFSE dilution assay (n = 4 –IL-1β and 7 +IL-1β mice/group): (**h**) experimental design, and (**i**) representative histograms and quantification of HSC^{LT} division kinetics. (**j**) Representative histograms, PU.1 levels and frequency of PU.1$^+$ HSCs from *PU.1-eYFP* mice injected ± IL-1β for 1 or 20 days (n = 4 –IL-1β and 5 +IL-1β mice/group for day 1; n = 5 –IL-1β and 3 +IL-1β mice/group for day 20). (**k**) Fluidigm gene expression analyses of myeloid determinants in HSCs from mice injected ±IL-1β for 20 days (n

= 8 pools of 100 cells for each condition; bars: means). Results are expressed as fold changes compared to levels in -IL-1β HSCs (set to 1). Source data for **i** and **j** are shown in Supplementary Table 1. Data are means ± S.D.; */° $p \leq 0.05$, **$p \leq 0.01$, ***$p \leq 0.001$. *P*-values in **b-k** were determined by Mann-Whitney *u* test and in **b** (relative to day 0) by one-way ANOVA with Dunnet's test. Exact *P*-values, number of replicates used to derive statistical data (n), and statistical tests used are shown in Supplementary Table 2.

Figure 5 | IL-1 accelerates myeloid regeneration following acute BM injury. (**a**) Experimental design and IL-1α/β levels following 5-FU treatment (n = 6 mice/group, day 0; n = 5 mice/group, day 8-10; n = 4 mice/group, day 12; n = 3 mice/group, day 14). (**b**) qRT-PCR analysis of *Il1a/b* expression in the indicated populations (n = 8 pools of 100 OBC, MSC and EC/group; n = 6 pools of 100 cells for all other populations). Results are expressed as fold changes compared to levels in B cells or d0 populations (each set to 0). (**c**) Experimental design and complete blood counts in 5-FU-treated $Il1r1^{+/+}$ and $Il1r1^{-/-}$ mice (n = 5 $Il1r1^{+/+}$ and 6 $Il1r1^{-/-}$ mice/group). **d-g** Engraftment of $Il1r1^{+/+}$ and $Il1r1^{-/-}$ HSCs isolated from mice 10 days post-5-FU treatment: (**d**) experimental design, (**e**) donor chimerism and (**f**) donor myeloid (Mac-1^+Gr-1^+) and lymphoid ($B220^+$ or $CD3^+$) lineage distribution in PB over time, and (**g**) donor chimerism in BM HSCs 16 weeks post-transplant. Source data for **a** and **e-g** are shown in Supplementary Table 1. Data are means ± S.D.; * $p \leq 0.05$, **$p \leq 0.01$. *P*-values in **a** and **b** were determined by one-way ANOVA with Dunnet's and Tukey's tests, respectively, and in **c-g** by Mann-Whitney *u* test. Exact *P*-values, number of replicates used to derive statistical data (n) and statistical tests used are shown in Supplementary Table 2.

Figure 6 | Chronic IL-1 exposure forces myeloid cell production at the expense of HSC

engraftment. a-d, Short-term tracking of HSCs from mice injected ± IL-1β for 20 days and transplanted into sublethally irradiated (sub-IR) recipients injected ± IL-1β for another 30 days (n = 9 +IL-1β and 10 -IL-1β mice/group): (**a**) experimental design, (**b**) donor chimerism in PB over time (°$p < 0.05$, °°$p < 0.01$ *vs.* -IL-1β recipients), (**c**) lineage distribution in PB, and (**d**) donor chimerism in BM HSCs (circles: individual mice, black lines: mean values) 30 days post-transplant. **e-g,** Short-term tracking of lentivirus-transduced PU.1-overexpressing HSCs (n = 4 ctrl and 5 PU.1 mice/group): (**e**) experimental design, (**f**) donor chimerism in PB over time, and (**g**) donor chimerism in BM HSCs (circles: individual mice, black lines: mean values) 30 days post-transplantation. Source data for **f** and **g** are shown in Supplementary Table 1. Data are means ± S.D.; * $p \leq 0.05$, ** $p \leq 0.01$, *** $p \leq 0.001$. *P*-values in **b** and **d** were determined by one-way ANOVA with Tukey's test, in **c** and **g** by Mann-Whitney *u* test, and in **f** by Student's *t* test. Exact *P*-values, number of replicates used to derive statistical data (n) and statistical tests used are shown in Supplementary Table 2.

Figure 7 | Chronic IL-1 exposure impairs HSC self-renewal. a-c, Long-term engraftment of HSCs from mice injected ± IL-1β for 20 days and transplanted into lethally irradiated (IR) recipients (n = 10 mice/group): (**a**) experimental design, (**b**) donor chimerism and (**c**) lineage distribution in PB over time. **d-f,** Long-term engraftment of HSC^{LT} from mice injected ± IL-1β for 70 days (n = 9 -IL-1β and 10 +IL-1β mice/group): (**d**) experimental design, (**e**) donor chimerism and (**f**) lineage distribution in PB over time. **g-i,** Secondary transplantation (2° txpl) of HSCs re-isolated from primary transplanted mice (1° txpl, shown in a) reconstituted with HSCs from mice injected ± IL-1β for 20 days (n = 8 mice/group): (**g**) experimental design, (**h**) donor chimerism and (**i**) lineage distribution in PB over time. Source data for **b-c**, **e-f**, and **h-i** are

shown in Supplementary Table 1. Data are means ± S.D.; * $p \leq 0.05$, ** $p \leq 0.01$, *** $p \leq 0.001$. *P*-values in **b**, **e**, **h** and **i** were determined by Mann-Whitney *u* test, and in **c** and **f** by Student's *t* test. Exact *P*-values, number of replicates used to derive statistical data (n) and statistical tests used are shown in Supplementary Table 2.

Figure 8 | IL-1 effects are reversible upon withdrawal. a-d, Analysis of mice injected ± IL-1β for 20 days and subsequently rested (R) for 8 weeks (n = 5 mice/group): (**a**) experimental design, (**b**) PB parameters, (**c**) progenitor cell, and (**d**) HSC^{LT} and MPP1 numbers. **e-f**, Long-term engraftment of HSCs from mice injected ± IL-1β for 20 days and rested for 8 weeks (n = 4 -IL-1β and 5 +IL-1β mice/group: (**e**) donor chimerism and (**f**) lineage distribution in PB over time. (**g**) Model for IL-1 effects on HSC function. At steady state, HSCs are essentially kept in a quiescent state that is geared towards maintenance of blood homeostasis. In this context, IL-1 is produced at low levels in the BM, primarily by granulocytes (Gr) and $CD4^+$ T cells and has minimal impact on HSC function. Upon infection or injury, IL-1 is produced at elevated levels in the BM microenvironment, in particular by endothelial cells (EC) that form an essential component of the HSC niche, and thus can provide localized IL-1 signalling to HSC. In this context, IL-1 functions as an 'emergency' signal that directly instructs HSCs towards myeloid differentiation, via activation of the NF-κB pathway and engagement of a PU.1-dependent myeloid gene program resulting in accelerated cell division and precocious differentiation into myeloid progenitors and ultimately mature myeloid cells. While such a response is advantageous in the context of acute inflammation and blood regeneration, it is ultimately detrimental in situations of chronic exposure since IL-1 exposed HSCs lose their ability to differentiate into the lymphoid and erythroid lineages, and exhibit decreased self-renewal activity and regenerative

potential in response to replicative challenges such as transplantation. However, these damaging consequences are fully reversible upon IL-1 withdrawal, indicating that IL-1 effects are essentially transient and require continuous exposure to negatively impact HSC function. Source data for **b-f** are shown in Supplementary Table 1. Data are means ± S.D.; * $p \leq 0.05$. All *P*-values were determined by Mann-Whitney *u* test. Exact *P*-values, number of replicates used to derive statistical data (n) and statistical tests used are shown in Supplementary Table 2.

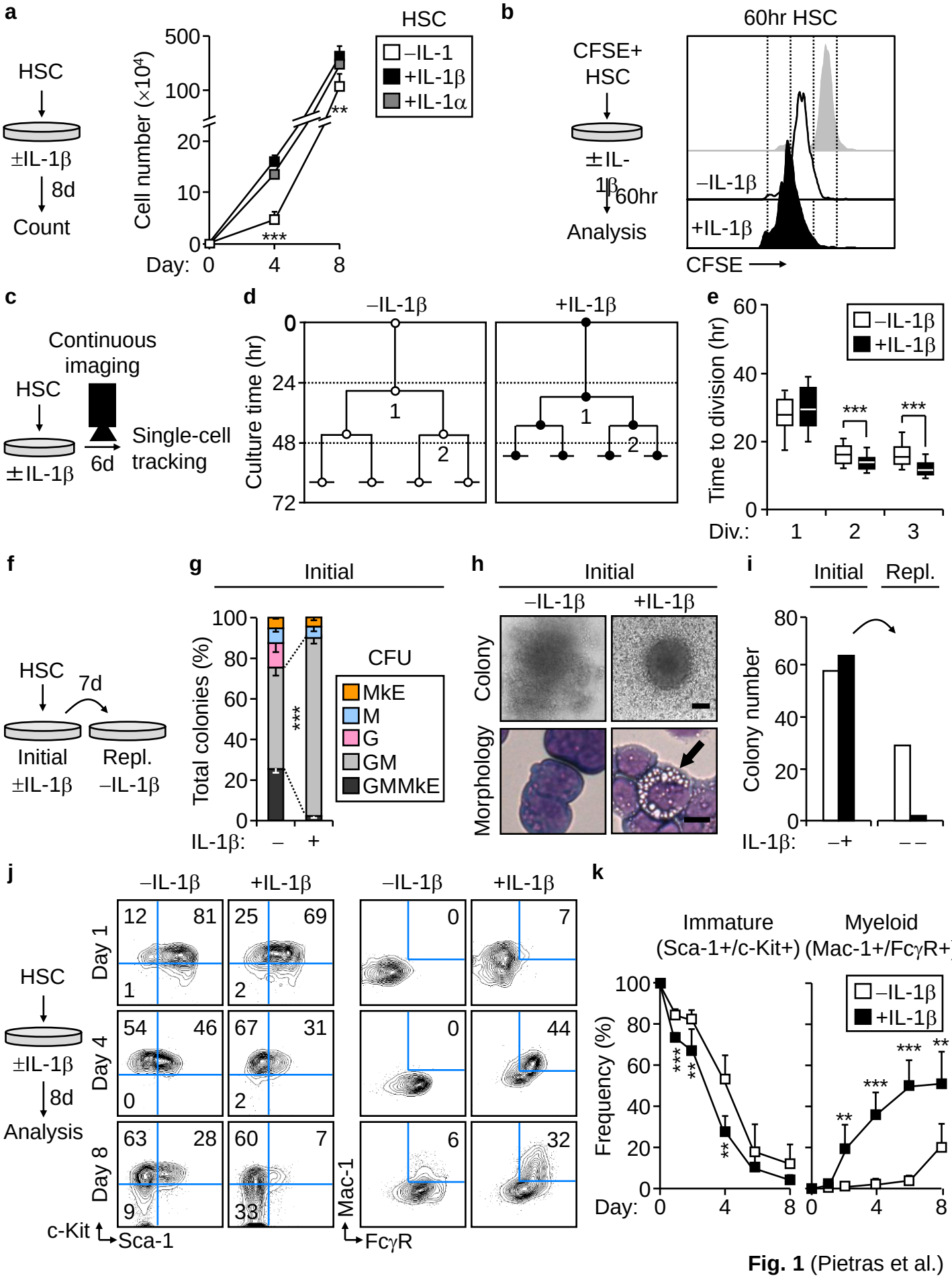

Fig. 1 (Pietras et al.)

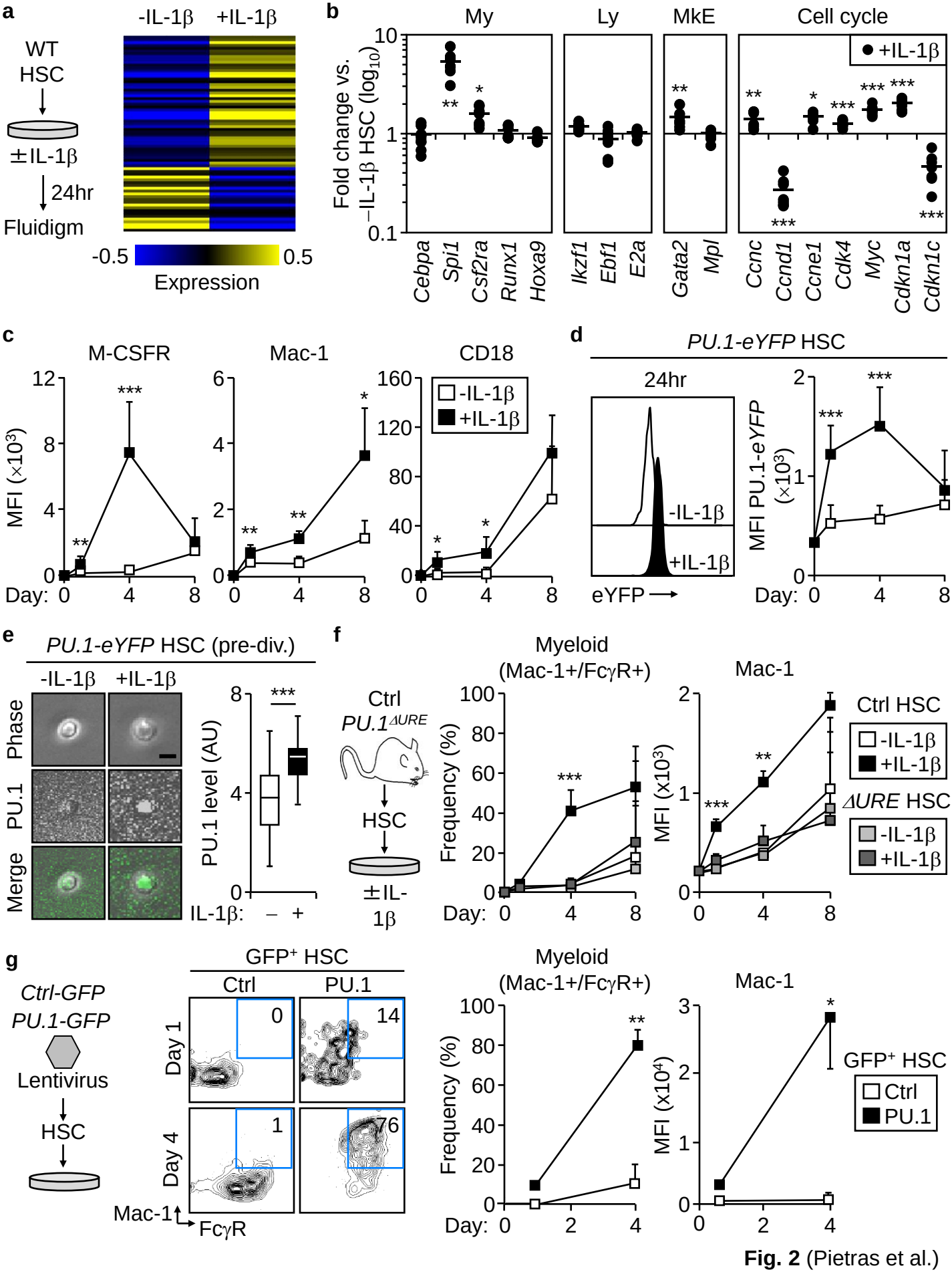

Fig. 2 (Pietras et al.)

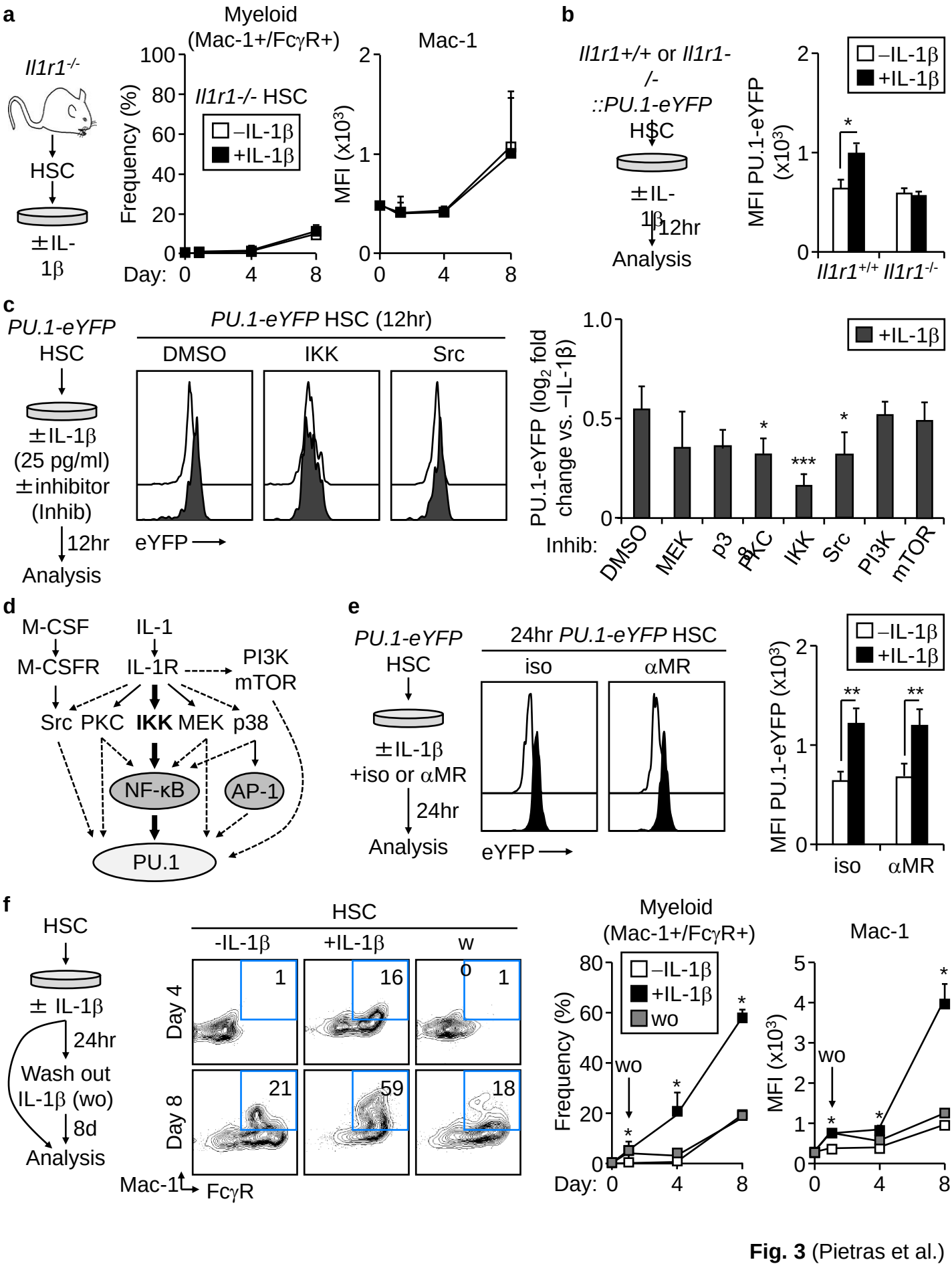

Fig. 3 (Pietras et al.)

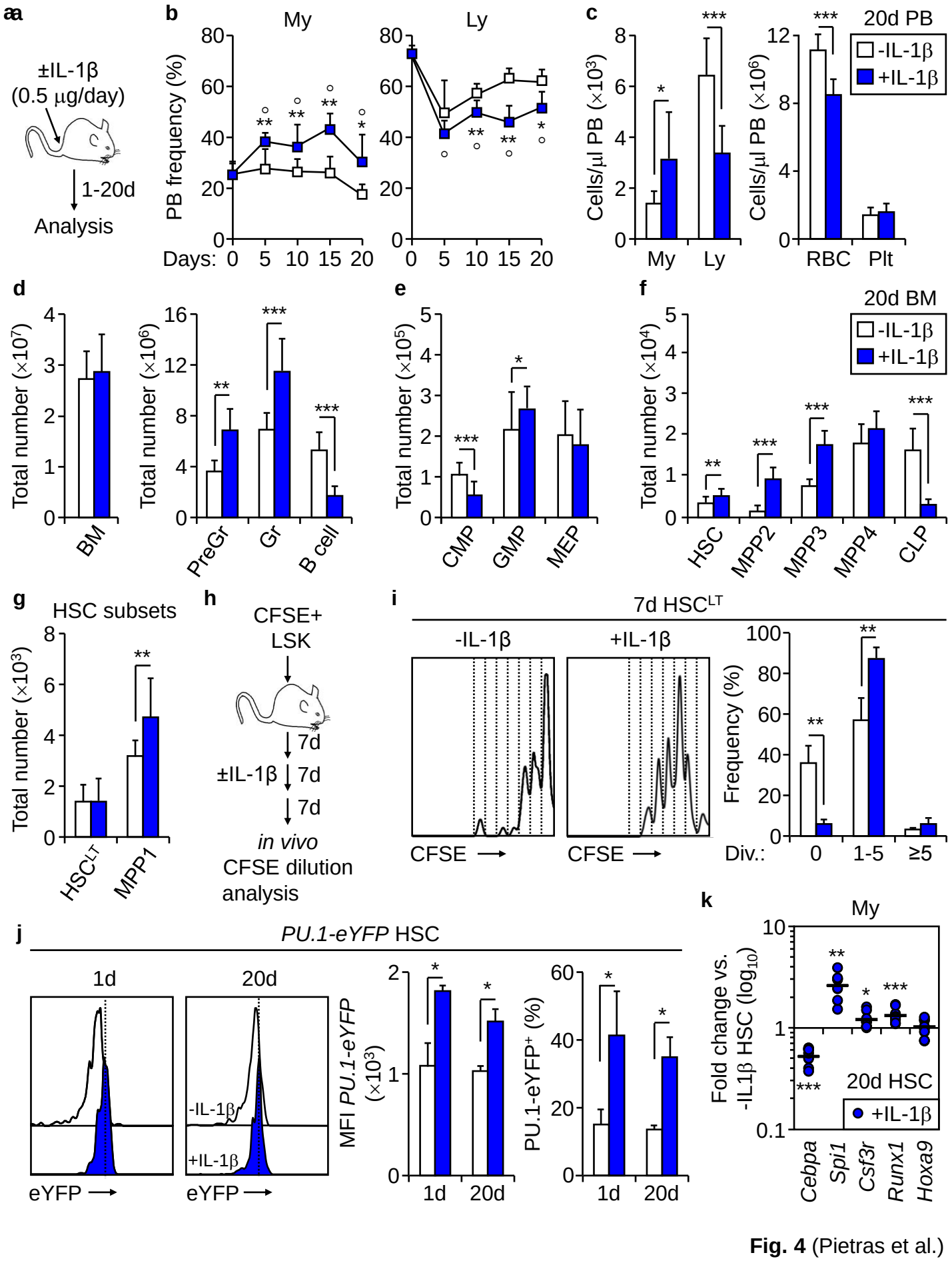

Fig. 4 (Pietras et al.)

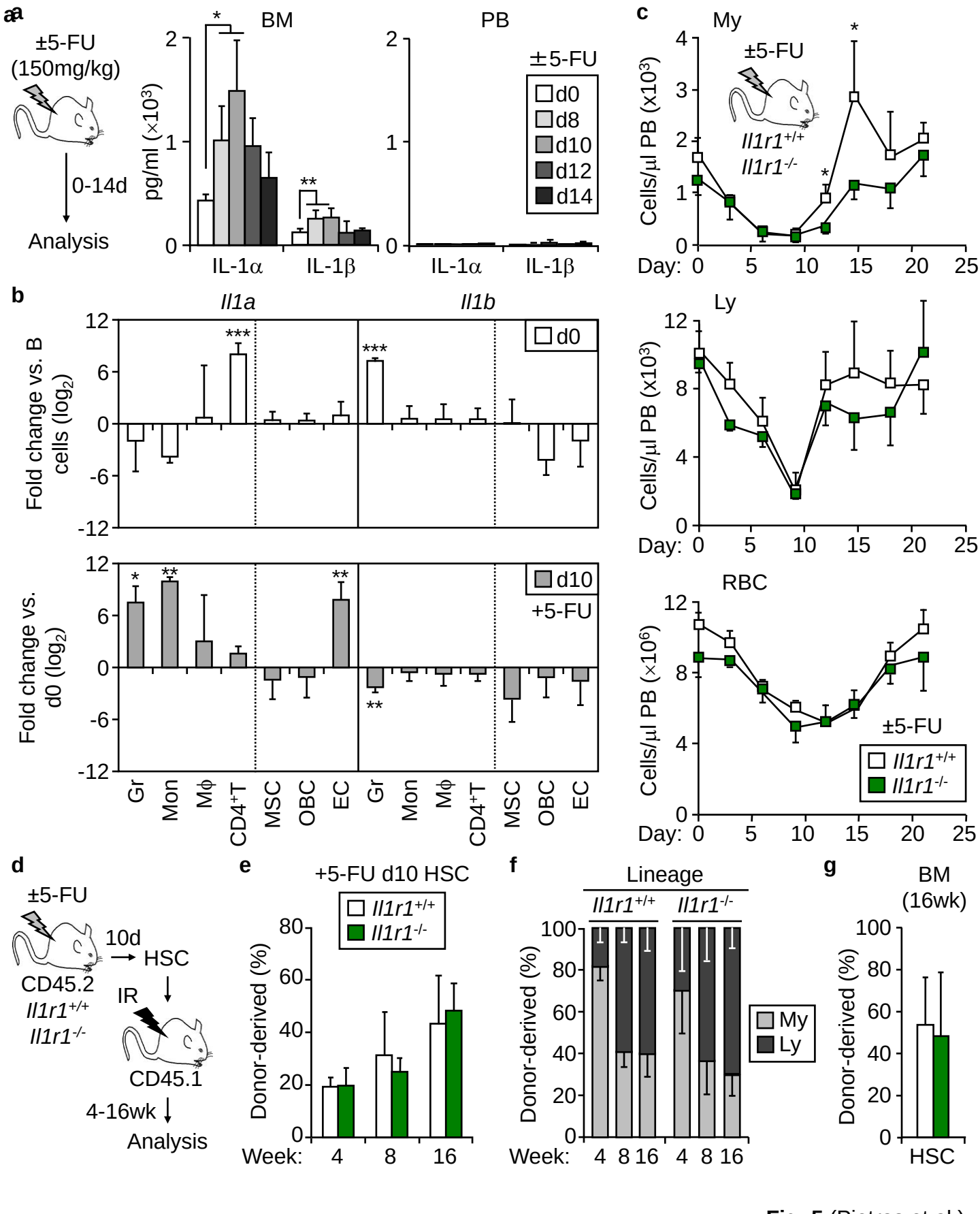

Fig. 5 (Pietras et al.)

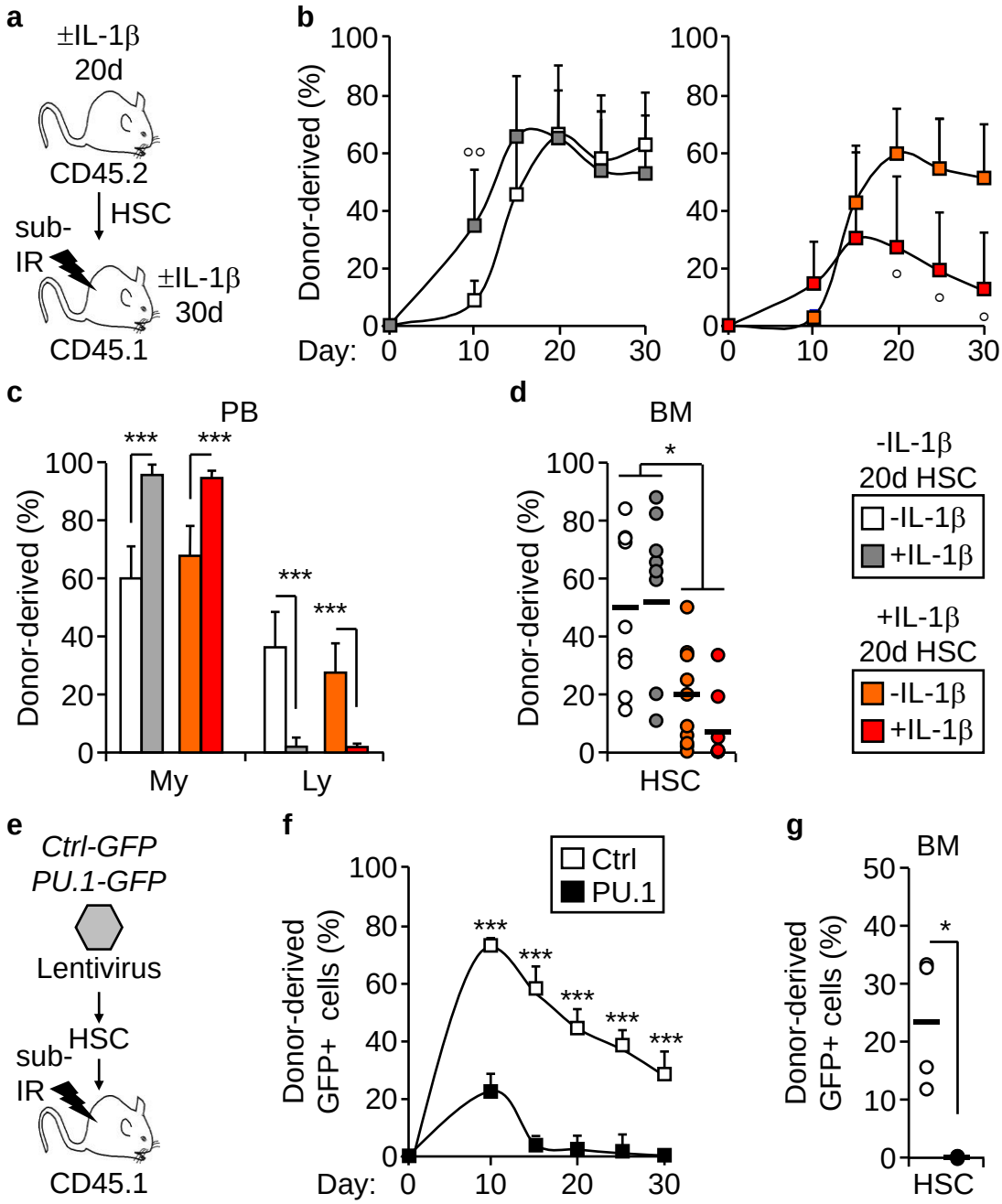

Fig. 6 (Pietras et al.)

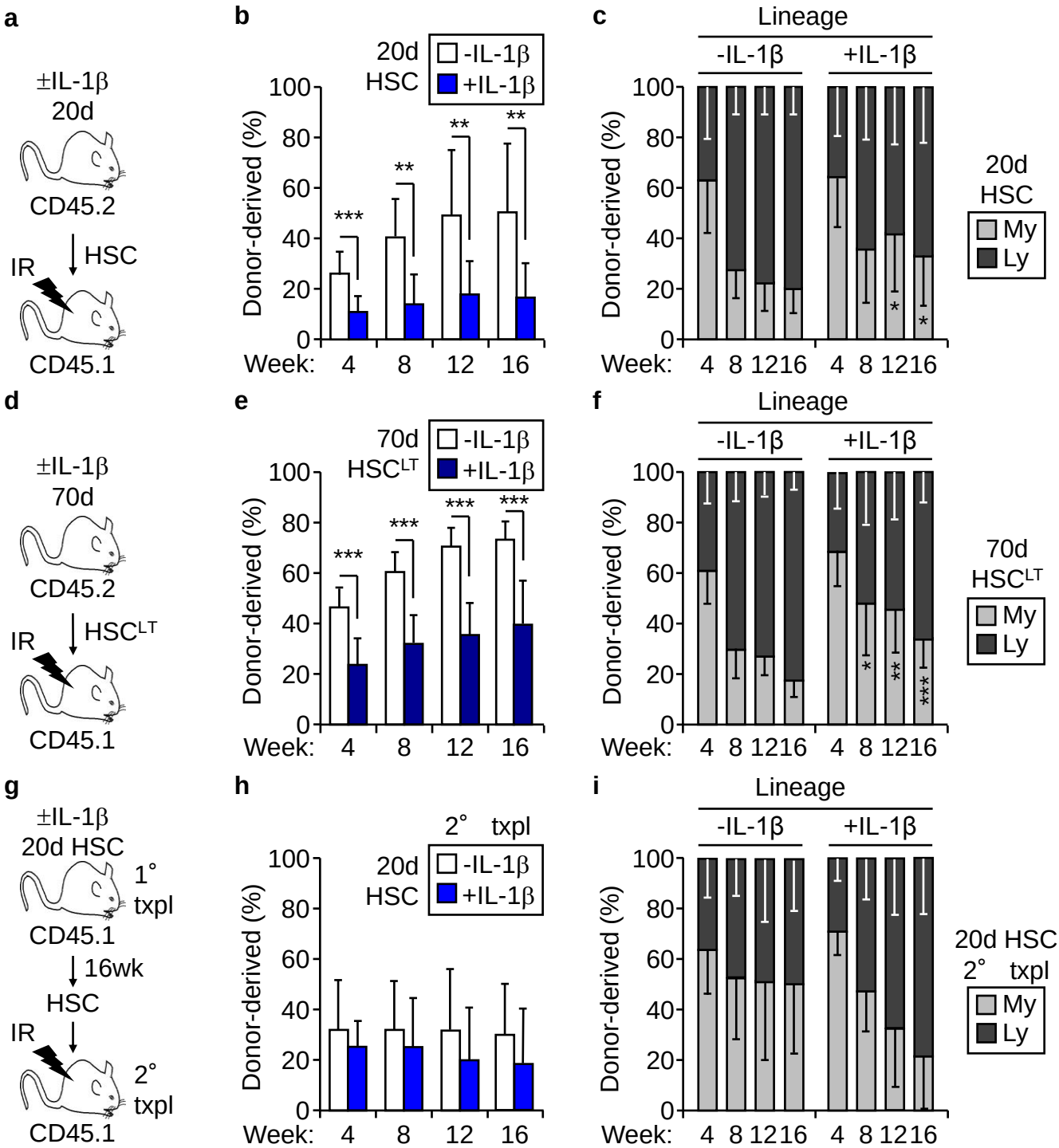

Fig. 7 (Pietras et al.)

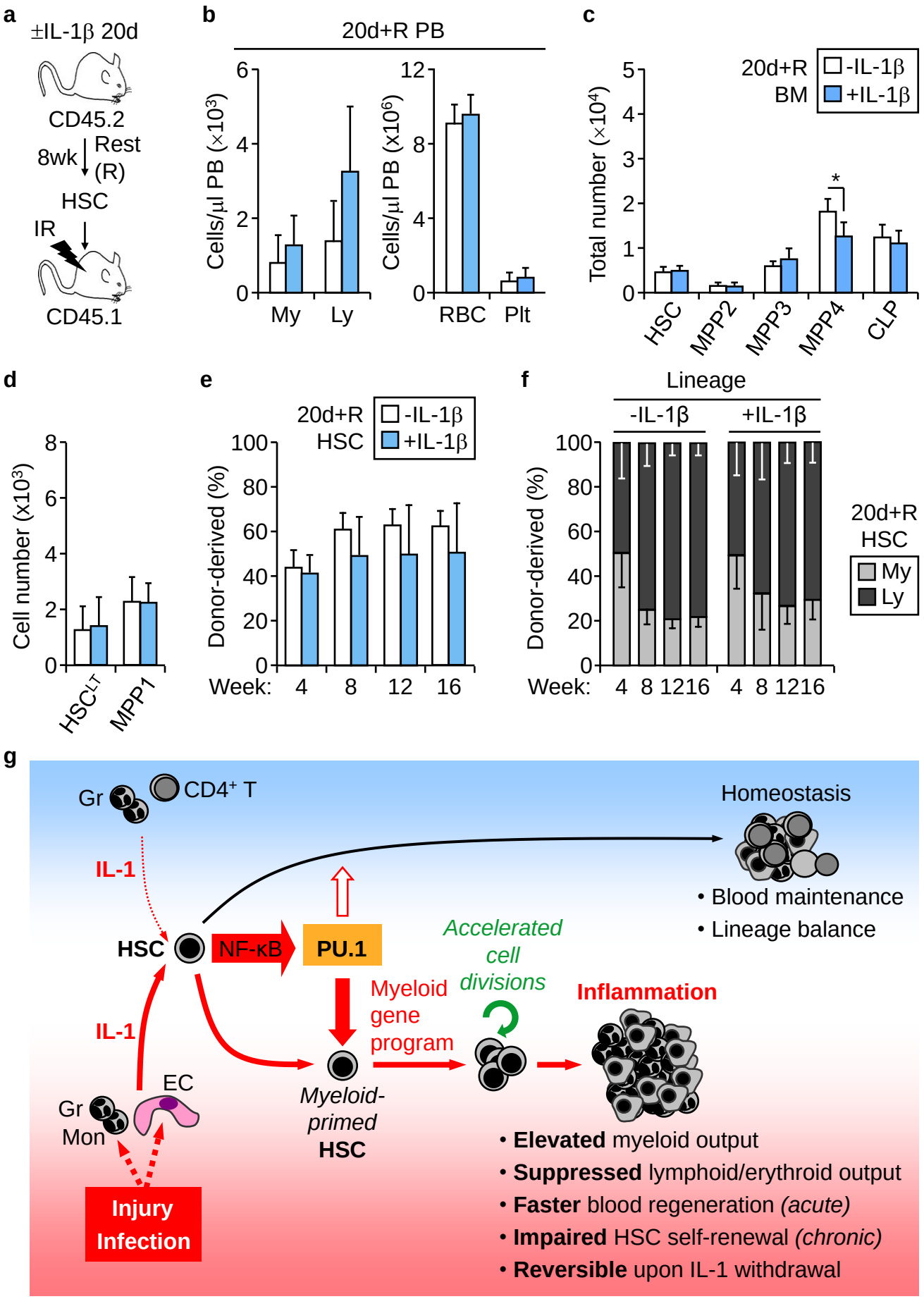

Fig. 8 (Pietras et al.)

ONLINE METHODS

Mice. Congenic wild type C57Bl/6 mice of both genders were bred in house and used for these studies. *Il1r1*$^{-/-}$ mice[40] and *PU.1-eYFP* mice (gift from Dr. C. Nerlov, Oxford University, UK) were on a pure C57Bl/6 background, while *PU.1ΔURE* mice[33] were on a mixed 129X1/SvJ × C57Bl/6 background. All experiments were performed in accordance with UCSF IACUC approved protocols.

***In vivo* assays.** For *in vivo* IL-1 treatment, mice were injected intraperitoneally (i.p.) with 0.5 μg IL-1β (Peprotech) in 100 μl PBS/0.2% BSA or 100 μl PBS/0.2% BSA alone once daily for up to 70 days in primary mice and 30 days in transplanted mice. For myeloablation treatment, mice were injected once i.p. with 150 mg/kg 5-fluorouracil (5-FU; Sigma-Aldrich) in PBS. For transplantation experiments, 8-12 week old CD45.1 C57Bl/6-Boy/J recipient mice were sublethally irradiated (9Gy, split dose 3hr apart) or lethally irradiated (11Gy, split dose 3hr apart) using a Cs^{137} source (J.L. Shepherd), and injected retro-orbitally with CD45.2$^+$ donor HSCs either alone following sublethal irradiation or together with 3×10^5 Sca-1-depleted BM cells following lethal irradiation. For transplantation experiments from 5-FU-treated mice, 500 HSCs were injected per lethally-irradiated recipient. For transplantation experiments from 20 days (with or without 8 week rest period) and 70 days IL-1-treated mice, 250 HSCs or HSC^{LT} were injected per lethally-irradiated recipient. For limiting dilution assays (LDA), 1×10^4, 1×10^5, or 1×10^6 unfractionated CD45.2$^+$ donor BM cells were combined with 2×10^5 CD45.1$^+$ competitor cells, and injected per lethally-irradiated recipient. For secondary transplantations, 500 HSCs were injected per lethally-irradiated recipient. For transplantation experiments in sublethally irradiated mice receiving ± IL-1β, 1000 HSCs were injected per recipient. For *in vivo* CFSE dilution assays, 1.0-1.1×10^5 CFSE-labelled CD45.2$^+$ LSK cells or 1.5×10^6 naïve T-cells were injected per non-irradiated CD45.1$^+$/CD45.2$^+$ F1 recipient. Mice were analysed 21 days after transplantation and the zero-divisional cell fraction was determined according to the CFSE intensity of naïve donor T-cells as described[36]. Irradiated mice were maintained on antibiotic-containing water for at least 4 weeks following transplantation, and analysed for donor-derived chimerism by regular bleeding. Peripheral blood (PB) was obtained from retro-orbital bleeding, and collected in 4 ml of ACK (150 mM NH_4Cl/10 mM $KHCO_3$) containing 10 mM EDTA for flow cytometry analyses, or in EDTA-coated tubes (Becton Dickenson) for complete blood count (CBC) analysis using a Hemavet 950 CBC analyser (Drew Scientific). HSC frequencies from LDA experiments were calculated using ELDA software (http://bioinf.wehi.edu.au/software/elda/)[56]. Engraftment was defined as ≥ 0.5% donor PB chimerism at 16 weeks post transplantation.

Flow cytometry. BM stem and progenitor populations were analysed and/or isolated as described[30]. For cell sorting, BM cells were obtained by crushing leg, arm and pelvic bones from mice in Hanks' Buffered Saline Solution (HBSS) containing 2% heat-inactivated FBS. Erythrocytes and contaminating bone cells were removed by ACK lysis followed by centrifugation on a Ficoll gradient (Histopaque 1119, Sigma-Aldrich). BM was subsequently enriched for c-Kit$^+$ cells using c-Kit microbeads (Miltenyi Biotec, 130-091-224) and an AutoMACS cell separator (Miltenyi Biotec). For population analyses, BM cells were flushed

from one tibia and one femur per mouse and cellularity was determined using a ViCell automated cell counter (Beckman-Coulter). For wild-type mice, cells were incubated with purified, unconjugated lineage antibodies against CD3 (BioLegend, 100202), CD4 (eBioscience, 16-0041-82), CD5 (eBioscience, 14-0051-85) CD8 (eBioscience, 16-0081-82) B220 (eBioscience, 16-0451-82) Ter119 (eBioscience, 16-5921-85), Mac-1 (eBioscience, 16-0112-85) and Gr-1 (eBioscience, 14-5931-85), followed by goat anti-rat-PE-Cy5 (Invitrogen, A10691), subsequently blocked with purified rat IgG (Sigma-Aldrich) and stained with c-Kit APC-eFluor780 (eBioscience, 47-1171-82), Sca-1-PB (BioLegend, 108120), Flk2-Bio (eBioscience, 13-1351-82), CD48-A647 (BioLegend, 103416), CD150-PE (BioLegend, 115904), FcγR-PerCP-eFluor710 (eBioscience, 46-0161-82), CD34-FITC (eBioscience, 11-0341-85) and either SA-PE-Cy7 (eBioscience, 25-4317-82) or SA-Qdot605 (Invitrogen, Q10101MP). For identification of $CD41^+$ HSC, a staining including Lin/PE-Cy5, c-Kit-APC-eFluor780, Sca-1-PB, CD48-A647, CD150-PE-Cy7 (BioLegend, 115913), CD34-Bio (BioLegend, 119304) followed with SA-Qdot605, CD41-FITC (eBioscience, 11-0411-82) and CD229-PE (BioLegend, 122905). For identification of CLP, a separate staining including Lin/PE-Cy5, c-Kit-APC-eFluor780, Sca-1-PB, Flk2-Bio/SA-Q-dot605 and IL7R-PE-Cy7 (eBioscience, 25-1271-82) was performed. For *PU.1-eYFP* mice, two separate stains were performed, one including CD150-PE, CD48-A647 and Flk2-Bio/SA-PE-Cy7, and the second one FcγR-PerCP-eFluor710 and CD34-Bio followed with SA-Qdot605 alongside Lin/PE-Cy5, c-Kit-APC-eFluor780 and Sca-1-PB. For sorting HSCs from IL-1 or 5-FU-treated mice, CD34 and FcγR were excluded and Mac-1 was stained separately from the lineage markers using Mac-1-PE-Cy7 (eBioscience, 25-0112-82) to control for potential increases in expression caused by IL-1, and HSC purity was further verified by inclusion of ESAM-FITC (Biolegend, 136205). Stromal BM EC, MSC and OBC were isolated from hematopoietic-depleted, collagenase-treated bone chips as described[40] using Lin/PE-Cy5, Sca-1-PB, CD45-APC-Cy7 (BD Biosciences, 557659), CD31-FITC (BD Biosciences 558738) and CD51-Bio (BD Biosciences 551380) followed by SA-APC (eBioscience 17-4317-82). BM granulocytes ($Mac\text{-}1^+Gr\text{-}1^{hi}M\text{-}CSFR^-$), pre-granulocytes ($Mac\text{-}1^+Gr\text{-}1^{int}Ly6C^{lo}$), monocytes ($Mac\text{-}1^+Ly6C^+M\text{-}CSFR^+F4/80^-$) and macrophages ($Mac\text{-}1^+Gr\text{-}1^{lo}M\text{-}CSFR^+F4/80^+SSC^{int/lo}$) were identified and isolated as described[57] using Mac-1-PE-Cy7, Gr-1-PB (eBioscience, 57-5931-82), Ly6C-PE-Cy5.5 (Biolegend, 128012), M-CSFR-Bio (eBioscience 13-1152-81) followed by SA-Qdot605, and F4/80-APC (eBioscience, 17-4801-82). BM B-cells ($B220^+CD19^+$), $CD4^+$ T cells ($CD4^+$) and $CD8^+$ T cells ($CD8^+$) were identified and isolated using B220-APC-Cy7 (eBioscience, 47-0452-82), CD19-PE (eBioscience, 12-0193-82), CD3-APC (eBioscience, 17-0032-82), CD4-FITC (BD Biosciences, 553729), and CD8-PE (Biolegend, 100908). For assessing myeloid differentiation in cultures, the same c-Kit-APC-eFluor780, Sca-1-PB, FcγR-PerCP-eFluor710 and Mac-1-FITC (eBioscience 11-0112-82) were used, plus either M-CSFR-Bio/SA-Qdot 605 or CD18-Bio (BD Biosciences, 557439) followed by SA-PE-Cy7, in separate stains. For transplantation experiments, donor and recipient cells were distinguished using CD45.1-FITC (eBioscience, 11-0454-85) and CD45.2-PE (eBioscience, 12-0453) with Mac-1-PE-Cy7, Gr-1-PB, CD3-APC, and B220-APC-Cy7 to assess lineage reconstitution in PB and BM, and CD45.1-FITC and CD45.2-PE-Cy7 (eBioscience, 25-0453-82) with c-Kit-eFluor780, Sca-1-PB, Flk2-Bio/SA-Qdot605, CD48-APC, and CD150-PE to assess lineage reconstitution in HSCs. Stained cells were re-suspended in HBSS/2% FBS and 1 μg/ml propidium idodide (PI) to exclude dead cells. For CFSE dilution assays, cells were stained with biotinylated lineage antibodies and enriched for Lin^- cells using anti-biotin microbeads (Miltenyi Biotec, 130-090-485) on MACS cell separation columns (Miltenyi Biotec), followed by SA-PB (Invitrogen,

S11222), c-Kit-PE-Cy5 (BioLegend, 105810) and Sca-1 APC-Cy7 (BioLegend, 108126). T-cells were enriched from spleen cells with a CD4-Bio (eBioscience, 13-0041-82) antibody and anti-biotin microbeads on MACS columns and subsequently stained with SA-PE-Cy5 (BioLegend, 405205) and CD62L-PE (eBioscience, 12-0621-81). Sorted LSK cells and $CD4^+CD62L^+$ naïve T-cells were subsequently labelled with 2μM CFSE (Molecular Probes) as described[34]. For analysis of CFSE-labelled donor cells following transplantation, cells were stained with biotinylated lineage antibodies and enriched as above, followed by SA-QDot 605, CD45.1-eFluor 450 (eBioscience, 48-0453-82), CD45.2-PerCP-Cy5.5 (eBioscience, 45-0454-82), c-Kit-PE-Cy7 (eBioscience, 25-1171-81) Sca-1-APC-Cy7 (BioLegend, 108126), FcγR-BV510 (BioLegend, 101333), CD150-PE, and CD34-A660 (eBioscience, 50-0341-80). Dead cells were excluded using Zombie Aqua™ Dye (BioLegend, 423102). For intracellular Ki67/DAPI staining, unfractionated BM cells were stained with Lin/PE-Cy5, c-Kit-APC-eFluor780, Sca-1-PE-Cy7 (BioLegend, 108113), CD150-PE and CD48-A647 and HSCs identified without Flk2, Isolated cells were washed in PBS, fixed with Cytofix/Cytoperm (BD Biosciences) for 30 min at 4°C, washed in Permwash, permeablized with Cytoperm Plus for 10 min at room temperature, washed again in Permwash, and stained with anti-Ki67-FITC (eBioscience, 11-5698-80) in Permwash for 2h at 4°C. Cells were washed with Permwash and re-suspended in PBS/3% FBS containing 1 μg/ml DAPI and incubated for 20 min prior to analysis. Cell isolation was performed on a FACSAria II or III (Becton Dickenson) using double sorting, and cell analyses were performed using a FACS LSR II (Becton Dickenson). Additional antibody information, including clones and dilutions, are listed in Supplementary Table 3.

Cell culture. All cultures were performed at 37°C in a 5% CO_2 water jacket incubator (Thermo Scientific). Cells were grown in StemPro34 medium (Invitrogen) supplemented with penicillin (50 U/ml)/streptomycin (50 μg/ml) and L-glutamine (2 mM), SCF (25 ng/ml), Flt3L (25 ng/ml), IL-11 (25 ng/ml), IL-3 (10 ng/ml), GM-CSF (10 ng/ml), Epo (4 U/ml) and Tpo (25 ng/ml) (Peprotech). IL-1α or IL-1β (Peprotech) was added at 25 ng/ml and M-CSF (Peprotech) at 100 ng/ml where indicated. For expansion assays, cells (400/well) were directly sorted into 96-well plates and cultured for up to 8 days. For surface marker tracking experiments, cells (2,500-5,000/well) were directly sorted into 96-well plates and cultured for up to 8 days. Cytokines were refreshed every other day by removing ~30% of the total well volume and replacing with fresh media, and cultures were split as needed. For cleaved caspase-3 and ATP activity assays, cells (400/well) were directly sorted into 384-well white luminescence culture plates containing 40 μl of media. Either directly after sorting or after 12hr an equal volume of Caspase-Glo 3/7 or CellTiter Glo substrate (Promega) was added to wells and the assay was performed according to manufacturer's instructions. For pathway blockade assays, HSC were cultured for 12h ± 25pg/ml IL-1β with either DMSO vehicle (1:1000 dilution) or 10 μm PD-0325901 (MEK inhibitor; Shanghai Chemokine Co., CAS 391210-10-9), 10 μm Rottlerin (PKC inhibitor; Tocris, 1610), 10 μm SB203580 (p38 inhibitor; Millipore, 559389), 10 μm BMS-345541 (IKK inhibitor; Sigma-Aldrich, B9935), 10 μm PP2 (Src inhibitor; Calbiochem, 529576), 50 μm LY294002 (PI3K inhibitor; Cell Signaling, 9901), and 200 μm Rapamycin (mTOR inhibitor; Sigma-Aldrich, R8781). For M-CSFR blocking assays, 10 μg/ml purified anti-M-CSFR (Biolegend, 135501) or Rat IgG2a isotype control (Biolegend, 400501) were added to the culture media. For colony formation assays, cells (100/1 ml/3 cm dish, or 1/100 μl/well of a 96-well plate) were cultured in methylcellulose (Stem Cell Technologies, M3231) supplemented with the above cytokines and

colonies were scored visually after 7 days. For serial replating, cells from primary methylcellulose cultures in 3 cm dishes were disaggregated and washed three times in PBS, and 1×10^4 cells were re-plated in fresh methylcellulose without IL-1β. For morphology analyses, 5×10^4 cells were spun directly onto glass slides using a Cytospin centrifuge (Beckman) and stained with Wright-Giemsa according to standard protocols. For BrdU incorporation assays, cells (5,000/well) were directly sorted into 96-well plates and cultured for 24hr in the presence of 60 μM BrdU (Sigma). Cells were then fixed in 4% paraformaldehyde in PBS for 20 min at room temperature, washed twice in PBS/50mM NH_4Cl, permeablized with 0.2% Triton-X in PBS, washed once in 0.2% PBS/3% BSA, incubated with anti-BrdU-APC (BD Biosciences, 51-23619L) for 30 min at room temperature, washed once more, re-suspended in 0.2% PBS/3% BSA and analysed on a FACS LSR II as described above. For CFSE dilution assays, cells (at least 5000 per point) were labelled with CFSE as previously described[58] and cultured for up to 60 hour before analyses.

Lentiviral transduction. Lentiviral transduction experiments were performed as previously described[59]. Filtered lentiviral supernatants were produced by the UCSF ViraCore facility from empty and PU.1-containing pCAD-GFP constructs[34] (gift from Dr. Ulrich Stiedl, Albert Einstein Medical College, New York, USA) with titers ranging from 1×10^6 to 4.5×10^6 infectious viral particles per ml. Freshly isolated HSCs were rested in StemPro medium without cytokines for 2hr and subsequently spin-infected with a 1:5 to 1:20 dilution of viral supernatant at 37°C for 90 min. Viral supernatants were removed and cells were cultured overnight (8-12 hours) in medium + cytokines. Spin-infection was repeated the next morning. GFP^+ transduced cells were analysed for myeloid surface marker expression starting 1 day after the last spinoculation.

Continuous single-cell tracking. HSCs isolated from *PU.1-eYFP* mice (200 per chamber) were cultured within fibronectin-pre-coated silicon chamber inserts (IBIDI, Martinsried, Germany) placed inside a sealed $25cm^2$ tissue culture flasks containing CO_2-saturated StemPro medium supplemented as described above, and 1 μg/ml custom-conjugated Sca-1-A647 and FcγR-A555 antibodies for continuous live staining by time-lapse microscopy as described[28]. Briefly, culture flasks were imaged on a Zeiss CellObserver system (Zeiss, Hallbergmoos, Germany) with a motorized stage and 37°C heated culture chamber. Phase-contrast images were obtained using a 10x objective (Zeiss) and recorded by an AxioCamHRm camera controlled with self-written Timm's Acquisition Tool (TAT) and Zeiss AxioVision 4.5 software. In addition, three fluorescence channels (YFP, A555 and APC) were acquired using mercury or xenon lamps. Phase-contrast images were acquired every 180 seconds, and fluorescence images for each channel every 240 minutes. Single-cell tracking analysis was performed using self-written Timm's Tracking Tool (TTT) software described previously[28]. Individual cells were manually analysed and annotated at each time frame for relevant features including division, apoptosis, and fluorescence, and data were subsequently stored as individual trees for each cell. HSCs were tracked for two subsequent generations (three total cell divisions). Rare apoptotic cells, or those with questionable identities or outlier division kinetics (*i.e.*, initial division shorter than 12h or longer than 48h), were excluded from the analyses. Cells undergoing endomitosis during the tracking period (*i.e.*, differentiating into megakaryocytes) were also excluded from the analyses. PU.1-eYFP reporter levels of bulk cells were automatically quantified from background-corrected fluorescence images at 0 and 15hr using self-written CAT software (T.S.,

unpublished). For individual tracked cells, *PU.1-eYFP* levels were quantified from fluorescence images of each tracked cell, acquired prior to the first division, using ImageJ software.

Gene expression. For direct qRT-PCR analysis, $1x10^4$ cells were cultured ± IL-1β for 12hr or isolated directly from IL-1-treated mice and resuspended into Trizol LS (Invitrogen). RNA was isolated according to the manufacturer's instructions, treated with DNase I (Invitrogen) and reverse-transcribed using a Superscript III kit (Invitrogen). 200 cell-equivalents of cDNA per sample were run in triplicate in 384-well qRT-PCR plates (Applied Biosystems) on an ABI 7900HT Fast Real-time PCR System (Applied Biosystems) using 2x Sybr Green master mix (Applied Biosystems). Ct values were normalized to *Gapdh* and relative changes were calculated using the ΔΔCt method. For Fluidigm gene expression analyses, pools of 100 cells were directly sorted per well of a 96-well plate containing 5ul of 2x CellsDirect reaction buffer (Invitrogen) and snap-frozen on dry ice until use. RNA was reverse-transcribed using Superscript III (Invitrogen) and subjected to 18 rounds of pre-amplification using a custom-designed set of target-specific primers as described[30]. Pre-amplification products were subsequently treated with Exonuclease I (New England Biolabs) to remove excess primers and diluted in DNA dilution buffer (Clontech). Pre-amplified cDNAs and custom-designed primer sets were loaded onto a Fluidigm 96.96 Dynamic Array IFC and run on a BioMark System (Fluidigm) using SsoFast Sybr Green for detection (BioRad). Data were analysed using Fluidigm software and normalized to *Gusb* expression. For analysis of *Il1a* and *Il1b* expression, pools of 100 cells were directly sorted into 2x CellsDirect reaction buffer and pre-amplified as described above, and 1µl of pre-amplified cDNA per sample was run in triplicate in 384-well qRT-PCR plates using KAPA Fast Sybr Green Master Mix (KAPA Biosystems) on the ABI 7900HT Fast Real-time PCR System. Ct values were normalized to *B-actin* and relative changes were calculated using the ΔΔCt method. Primer information, including sequences and NCBI gene IDs, are included in Supplementary Table 4.

Cytokine analyses. For PB serum, blood was harvested from euthanized mice via cardiac puncture, allowed to coagulate at room temperature for 30 min, and subsequently spun down at 12,000 × g for 10 min to remove blood cells. For BM plasma, the four long bones (two femurs and two tibiae) of the same mice were flushed with 150-200 µl HBSS/2% FBS using a 0.3cc insulin syringe with a 28g needle and spun at 500 × g for 5 min to remove BM cells. Supernatants were further clarified by spinning down at 12,000 × g for 10 min, and samples were subsequently stored at -20°C until use. For cytokine measurement, 50 µl of 2x-diluted sample was analysed with a Luminex Cytokine Mouse 20-plex panel (Life Technologies) using a BioPlex instrument (Bio-Rad) according to the manufacturer's instructions. M-CSF levels were analysed using an antibody sandwich ELISA kit (Raybiotech) according to the manufacturer's instructions.

Statistics and reproducibility. All experiments were performed in triplicate and repeated as indicated. *N* indicates the numbers of independent experiments performed. For *in vivo* experiments, sample sizes were predetermined based on estimation of the minimum number of animals required to obtain biologically meaningful results (at least 80% power). For other experiments no statistical method was used to predetermine sample size, and replicate

experiments were performed based on the variability of results obtained, as well as experiment type. Data were expressed as mean ± standard deviation (S.D.). Statistical analyses were performed using Prism 5.0 software (GraphPad). Pairwise statistical significance was evaluated by two-tailed Mann-Whitney *u*-test or Student's *t*-test. Statistical significance between multiple groups was evaluated by one-way ANOVA with Dunnet's or Tukey's test for multiple comparisons. The experiments were not randomized. The investigators were not blinded to allocation during experiments and outcome assessment. *P*-values ≤ 0.05 were considered statistically significant. Source data are provided in Supplementary Table 1. Exact *P*-values and statistical tests used are shown in Supplementary Table 2.

56. Hu, Y. & Smith, K. (2009). ELDA: Extreme limiting dilution analysis for comparing depleted and enriched populations in stem cell and other assays. *J Immunological Methods* **346**, 70-78.

57. Chow, A. *et al*. Bone marrow CD169+ macrophages promote the retention of hematopoietic stem and progenitor cells in the mesenchymal stem cell niche. *J Exp Med* **208**, 261-271 (2011).

58. Mohrin, M. *et al*. Hematopoietic stem cell quiescence promotes error-prone DNA repair and mutagenesis. *Cell Stem Cell* **7**, 174-185 (2010).

59. Flach, J. *et al*. Replication stress is a potent driver of functional decline in ageing haematopoietic stem cells. *Nature* **512**, 198-202 (2014).

SUPPLEMENTARY FIGURE LEGENDS

Supplementary Figure 1 | Gating strategy and effect of IL-1 on progenitor cell proliferation and survival. (**a**) Gating strategy and representative FACS plots of stained c-Kit-enriched wild-type (WT) BM cells. MPP2 and MPP3 are often isolated as a combined MPP2/3 population for experiments. (**b**) *Il1r1* expression in the indicated populations. Results are dye intensity levels from microarray analyses[30]. (n = 5 MPP4, n = 4 HSC and GMP, remainder n = 3). (**c**) Representative expansion in liquid culture in one of two independent experiments performed in triplicate. (**d**) Cleaved caspase-3 (CC3) activity expressed as relative luminescence units, RLU) after 12 hours culture in one of two independent experiments performed in triplicate (**e**) Experimental design and quantification of BrdU incorporation after 24 hours culture in one of two independent experiments performed in triplicate. (**f**) Mean absolute numbers of the indicated phenotypic cell populations in HSC cultures over time in two independent experiments. Source data for **b** are shown in Supplementary Table 1. Data are means, and shown in **b** as means ± S.D. Exact *P*-values, number of replicates used to derive statistical data (n) and statistical tests used are shown in Supplementary Table 2.

Supplementary Figure 2 | Effect of IL-1 on progenitor cell differentiation. a-b, Myeloid differentiation in cultured MPP2/3, MPP4 and GMPs: (**a**) representative FACS plots, and (**b**) quantification of surface marker expression (n = 4 biological replicates/group). (**c**) Single cell clonogenic colony forming unit (CFU) assays in methylcellulose (n = 60 cells/group). Colonies were scored after 7 days. MkE: megakaryocyte/erythrocyte; M: macrophage; G: granulocyte; GM: granulocyte/macrophage; GMMkE: mix colony. (**d**) Representative colony-type (scale bar, 100 μm) and colony-morphology (scale bar, 10 μm; arrows indicate macrophages). (**e**) Representative FACS plots of myeloid differentiation in cultured HSCs and GMPs (n = 3 biological replicates). Source data for **b** are shown in Supplementary Table 1. Data in **b** are means ± S.D.; * $p \leq 0.05$; *** $p \leq 0.001$. *P*-values in **b** were determined by Mann-Whitney *u* test. Exact *P*-values, number of replicates used to derive statistical data (n) and statistical tests used are shown in Supplementary Table 2.

Supplementary Figure 3 | PU.1 activation by IL-1. **a-b** qRT-PCR analyses of myeloid lineage genes the indicated populations after 12 hours culture (n = 4 biological replicates/group for HSC, MPP4 and GMP, n = 3 for MPP2/3): (**a**) experimental design, and (**b**) expression of individual genes. Results are expressed as fold changes compared to levels in each -IL-1β population (set to 0). (**c**) PU.1 levels in individual *PU.1-eYFP* HSCs at 0 and 15 hours culture (n = 140 and 186 individual HSC/group). Results are expressed in arbitrary units (AU) with box plots showing median (lines) and 10-90th percentile (whiskers). (**d**) Division kinetics of *PU.1-eYFP* HSCs from Fig. 1e re-analysed based on pre-division PU.1^{lo} (≤ 4 AU) and PU.1^{hi} (> 4 AU) expression levels. (**e**) Experimental design, representative histograms and quantification of BrdU incorporation in HSCs after 24 hours culture (n = 3 biological replicates/group). (**f**) PU.1 levels in *PU.1-eYFP* HSCs after 12 hours culture with the indicated concentrations of IL-1β. (**g**) Representative histograms showing PU.1 levels in *PU.1-eYFP* HSCs after 12 hours culture ± IL-1β (25 pg/ml) and the indicated inhibitors. Results with *Il1r1*$^{-/-}$*::PU.1-eYFP* HSCs are shown as negative controls. (**h**) Validation of the blocking activity of the anti-M-CSFR antibody (αMR) in BM cells

cultured for 5 days ± M-CSF (M, 100 ng/ml). Source data for **b** and **e** are shown in Supplementary Table 1. Data are means ± S.D.; * $p \leq 0.05$; *** $p \leq 0.001$. P-values in **b** and **e** were determined by paired Student's *t* test, and in **c-d** by one-way ANOVA with Tukey's test. Exact *P*-values, number of replicates used to derive statistical data (n) and statistical tests used are shown in Supplementary Table 2.

Supplementary Figure 4 | Gating strategies and effect of acute *in vivo* IL-1 treatment. a-c, Gating strategies with representative FACS plots for the different hematopoietic stem, progenitor and mature cell populations analysed in peripheral blood (PB) and bone marrow (BM): (**a**) PB of mice injected ± IL-1β for 20 days, (**b**) and (**c**) BM of mice injected ± IL-1β for 1 day. Number in each gate indicates population frequency. (**d**) BM cellularity and size of the indicated BM populations in mice injected ± IL-1β for 1 day (n = 15 –IL-1β and 13 +IL-1β mice/group). (**e**) Numbers of HSC^{LT} and MPP1 in $Il1r1^{+/+}$ and $Il1r1^{-/-}$ mice in mice injected ± IL-1β for 1 day (n = 15 -IL-1β and + IL-1β $Il1r1^{+/+}$ mice, 5 –IL-1β and 6 +IL-1β $Il1r1^{-/-}$ mice/group) Data are means ± S.D.; * $p \leq 0.05$; ** $p \leq 0.01$; *** $p \leq 0.001$. *P*-values in **d** and **e** were determined by Mann-Whitney *u* test. Exact *P*-values, number of replicates used to derive statistical data (n) and statistical tests used are shown in Supplementary Table 2.

Supplementary Figure 5 | *In vivo* HSC division tracking and specificity of PU.1 activation. (**a**) Representative FACS plots showing CFSE dilution in donor cells following 7 days treatment of the recipient mice ± IL-1β. (**b**) Gating strategy for identification of HSC^{LT} in CFSE-labelled donor cells. (**c**) PU.1 levels in the indicated populations from *PU.1-eYFP* mice injected ± IL-1β for 1 or 20 days (n = 4 –IL-1β and 5 +IL-1β_mice/group for day 1; n = 5 –IL-1β and 3 +IL-1β_ mice/group for day 20). Source data for **c** are shown in Supplementary Table 1. Data are means ± S.D.; * $p \leq 0.05$. P-values in **c** were determined by Mann-Whitney *u* test. Exact *P*-values, number of replicates used to derive statistical data (n) and statistical tests used are shown in Supplementary Table 2.

Supplementary Figure 6 | Cytokine production following 5-FU myeloablation, identification of IL-1 producing cells and haematopoiesis in $Il1r1^{-/-}$ mice. (**a**) Cytokine levels in BM plasma (top) and blood serum (bottom) of 5-FU-treated mice (mice/group: n = 7 day 0-8; n=8 day 10; n=6 day 12; n=3 day 14; for M-CSF n=4 day 0-12; n=3 day 14). (**b**) Experimental design and gating strategy used to isolate BM stromal ECs, MSCs and OBCs, and hematopoietic granulocytes (Gr), monocytes (Mon), macrophages (MΦ), B cells and CD4+ T cells. Representative FACS plots of untreated d0 mice are shown. (**c**) Representative FACS plots and quantification of Ki67/DAPI cell cycle distribution in HSCs from $Il1r1^{+/+}$ and $Il1r1^{-/-}$ mice (n = 4 $Il1r1^{+/+}$ and 6 $Il1r1^{-/-}$ mice/group). (**d**) BM cellularity and size of the indicated BM populations in $Il1r1^{+/+}$ and $Il1r1^{-/-}$ mice (n = 20 mice/group; for HSC^{LT} and MPP1, n = 16 $Il1r1^{+/+}$ and 13 $Il1r1^{-/-}$ mice/group) Source data for **a** are shown in Supplementary Table 1. Data are means ± S.D.; * $p \leq 0.05$; ** $p \leq 0.01$; *** $p \leq 0.001$. P-values in **a** were determined by one-way ANOVA with Dunnet's test, and in **c** and **d** by Mann-Whitney *u* test. Exact *P*-values, number of replicates used to derive statistical data (n) and statistical tests used are shown in Supplementary Table 2.

Supplementary Figure 7 | Short-term *in vitro* and *in vivo* tracking of HSCs. (**a**) Representative methylcellulose colony forming-unit (CFU) and cleaved caspase-3 (CC3; expressed as relative luminescence units: (RLU) assays. Results are representative of one of two independent experiments performed in triplicate. **b-c,** Terminal analyses of mice transplanted with HSCs exposed ± IL-1β for 20 days in donor mice and another 30 days in recipient mice shown in Fig. 6a-d): representative FACS plots showing donor chimerism, and myeloid (My) and lymphoid (Ly) donor lineage distribution in (**b**) PB and (**c**) BM HSCs 30 days post-transplant. (**d**) Representative FACS plots showing the frequency of GFP^+ control and PU.1-transduced HSCs prior to transplantation (d0 input) and after 30 days post-transplant in the BM (d30). Data in **a** are shown as means.

Supplementary Figure 8 | Functional analysis of IL-1-exposed HSCs. a-c, Limiting dilution analysis (LDA) of unfractionated BM cells from mice injected ± IL-1β for 20 days (10^6 cell dose: n = 4 –IL-1β and 4 +IL-1β mice/group; 10^5 cell dose: n = 4 mice/group; 10^4 cell dose: n = 4 –IL-1β and 3 +IL-1β mice/group): (**a**) experimental design, (**b**) LDA graph (values: estimated HSC frequency; solid lines: dose response curve; dashed lines: upper and lower confidence intervals), and (**c**) engraftment results at 16 weeks post-transplant, Mice with ≥ 0.5% donor chimerism were considered engrafted. **d-f,** Analyses of mice injected ± IL-1β for 70 days n = 5 mice/group): (**d**) representative FACS plots and HSC^{LT} number fractionated by CD41 expression (n = 4 –IL-1β and 5 +IL-1β mice/group), (**e**) size (means) of the indicated BM populations from two mice, and (**f**) methylcellulose colony forming-unit (CFU) assay in one experiment performed in triplicate. **g-i,** Secondary transplantation (2° txpl) of HSCs re-isolated from primary transplanted mice (1° txpl, shown in Fig. 7d-f) reconstituted with HSC^{LT} from mice injected ± IL-1β for 70 days (n = 5 mice/group): (**g**) experimental design, (**h**) donor chimerism and (**i**) lineage distribution in PB over time. Source data for **b-d** are shown in Supplementary Table 1. Data are means ± S.D. except when indicated. *P*-values in **b** were determined using Poisson statistical analysis, in **c**, **d**, **h** and **i** by Mann-Whitney *u* test. Exact *P*-values, number of replicates used to derive statistical data (n) and statistical tests used are shown in Supplementary Table 2.

SUPPLEMENTARY TABLE LEGENDS

Supplementary Table 1 | Statistics source data.

Supplementary Table 2 | Exact *p*-values and statistical tests used in experiments.

Supplementary Table 3 | Antibodies used.

Supplementary Table 4 | Primers used for qRT-PCR and Fluidigm analysis.

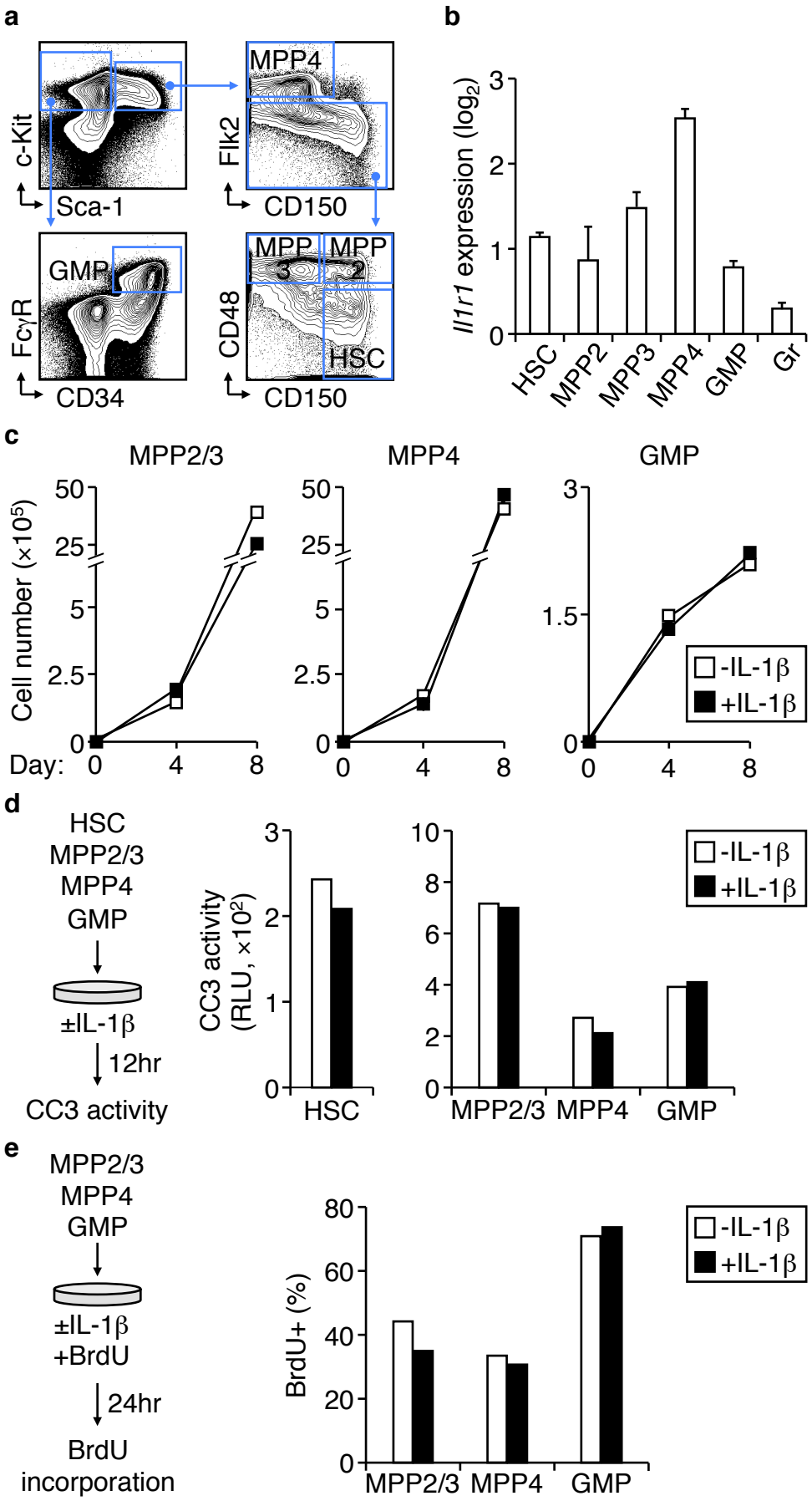

Fig. S1 (Pietras et al.)

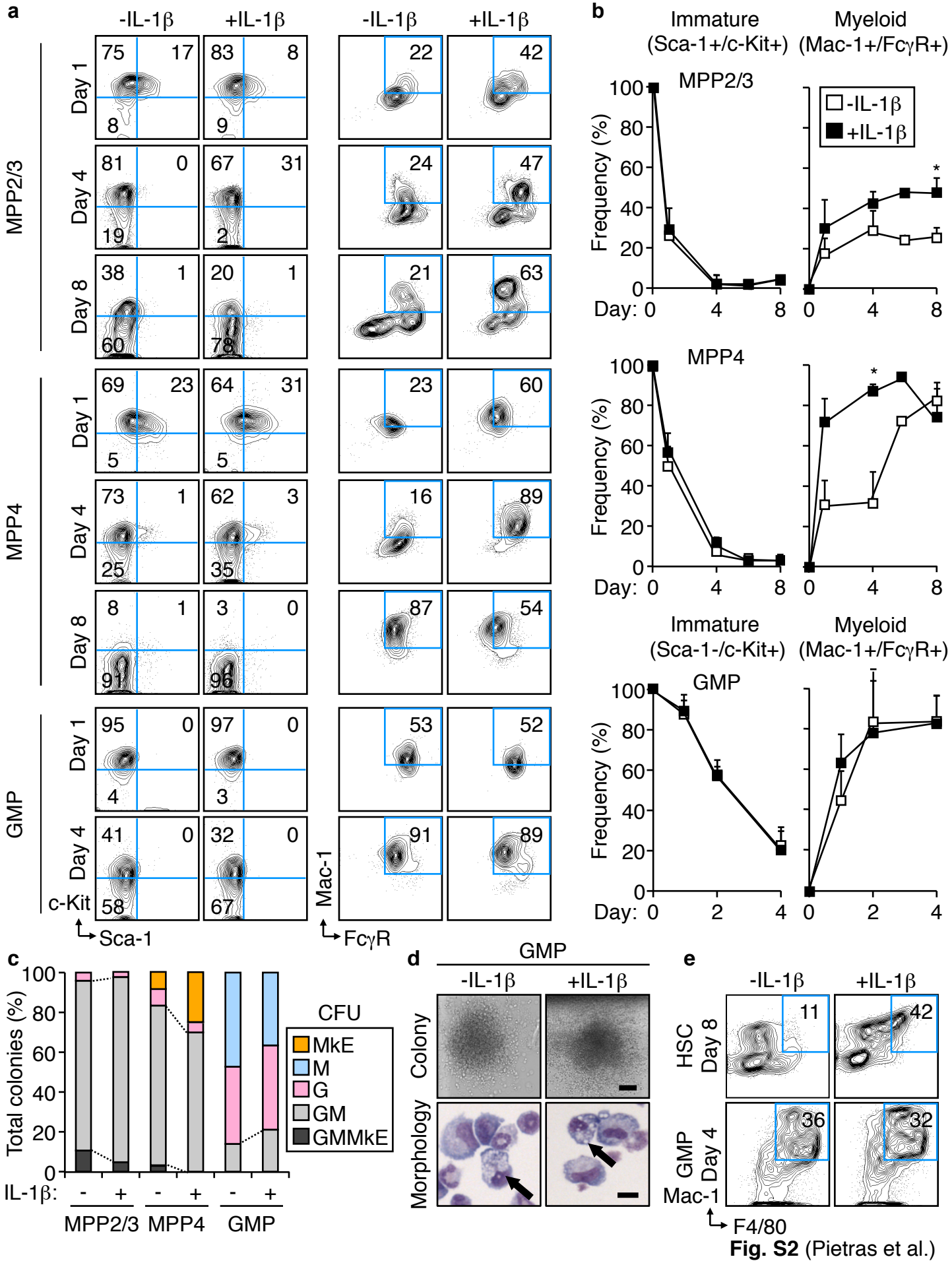

Fig. S2 (Pietras et al.)

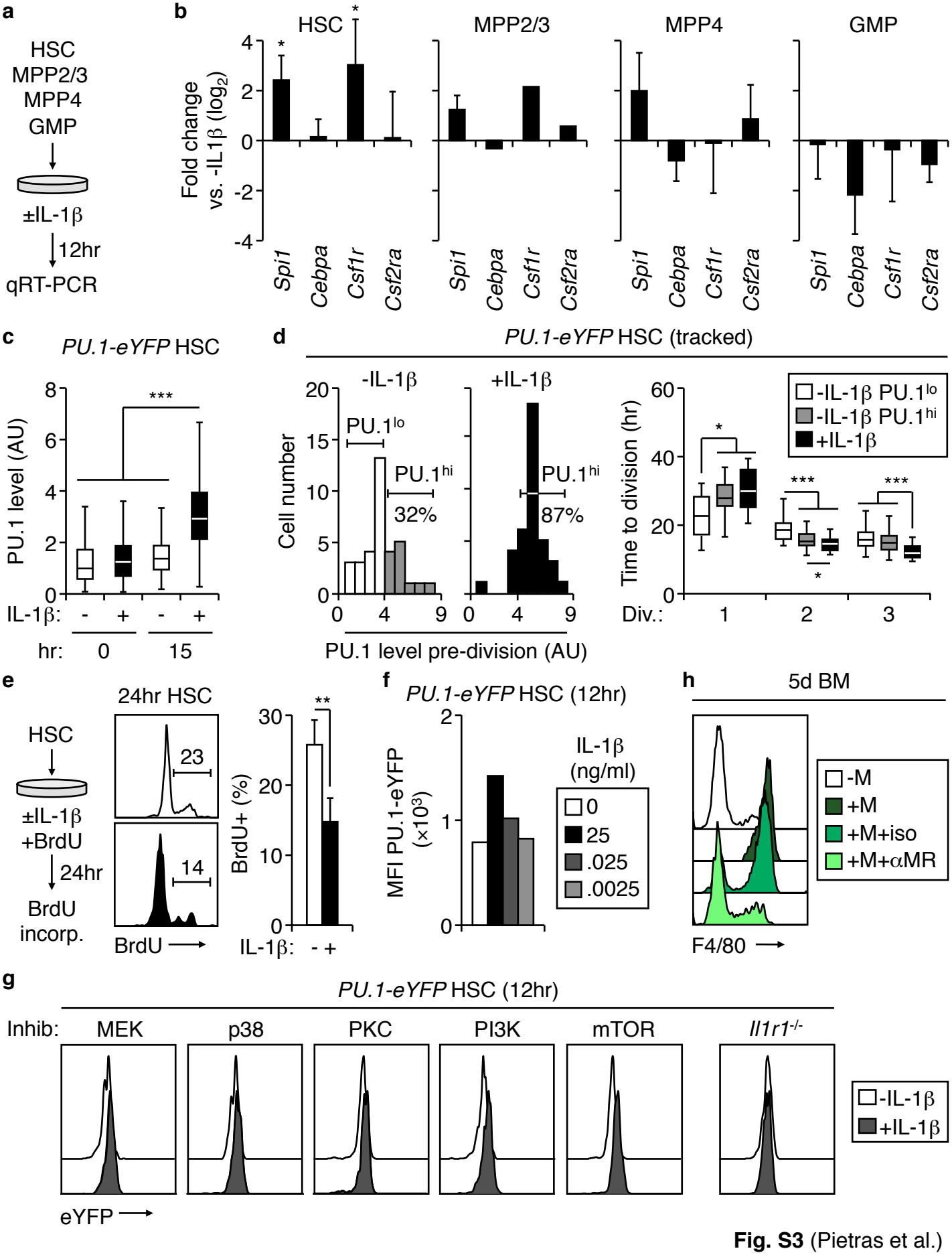

Fig. S3 (Pietras et al.)

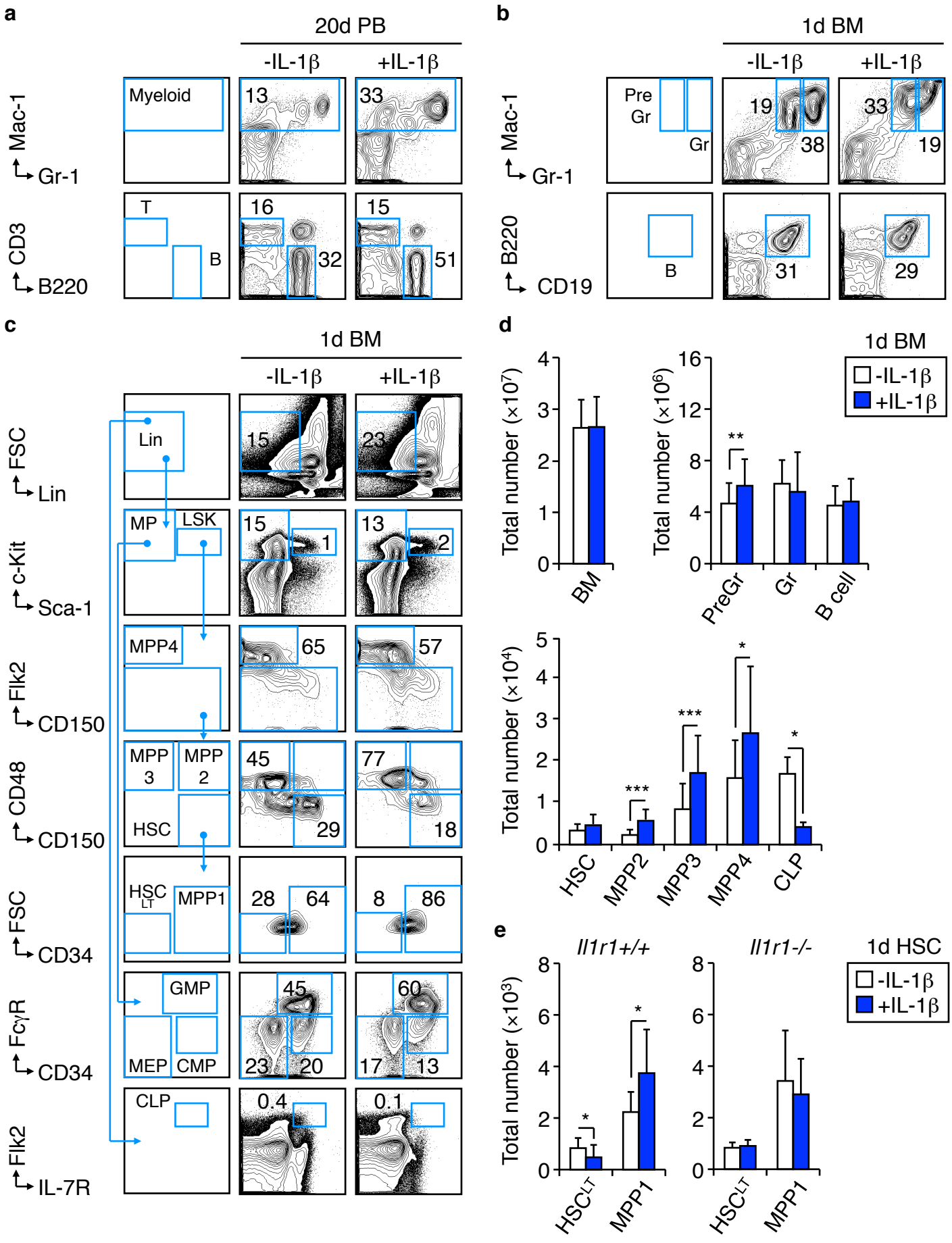

Fig. S4 (Pietras et al.)

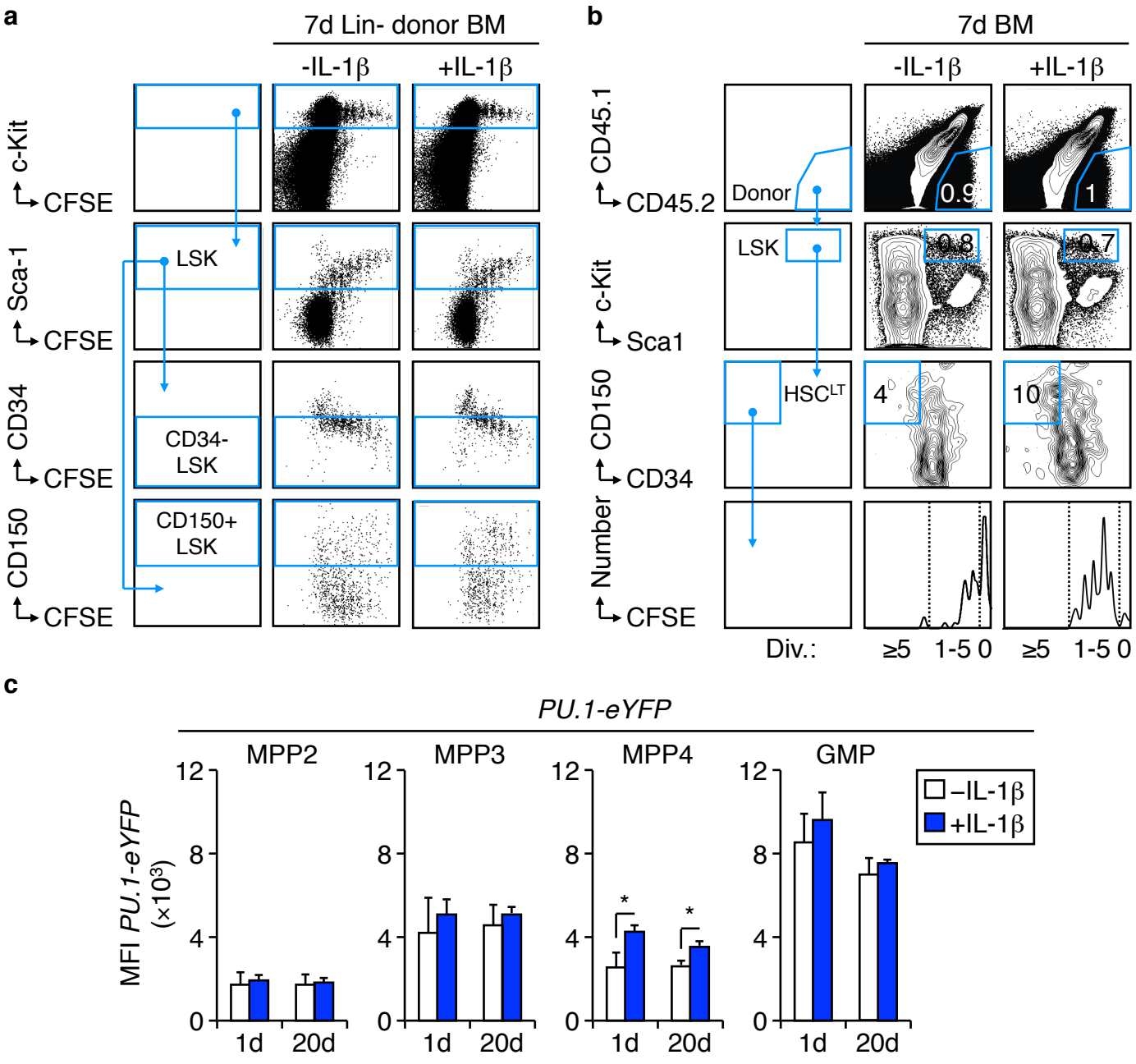

Fig. S5 (Pietras et al.)

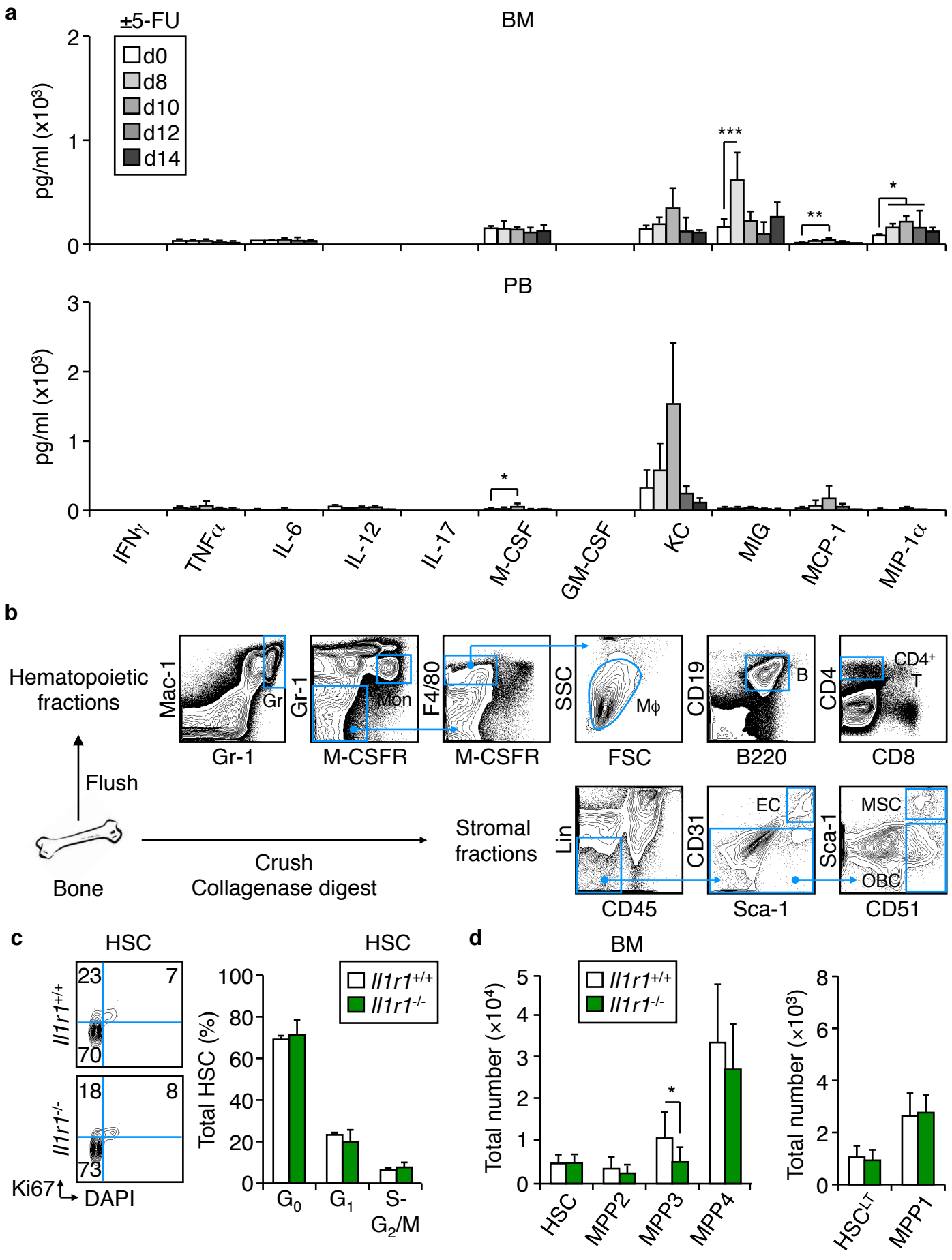

Fig. S6 (Pietras et al.)

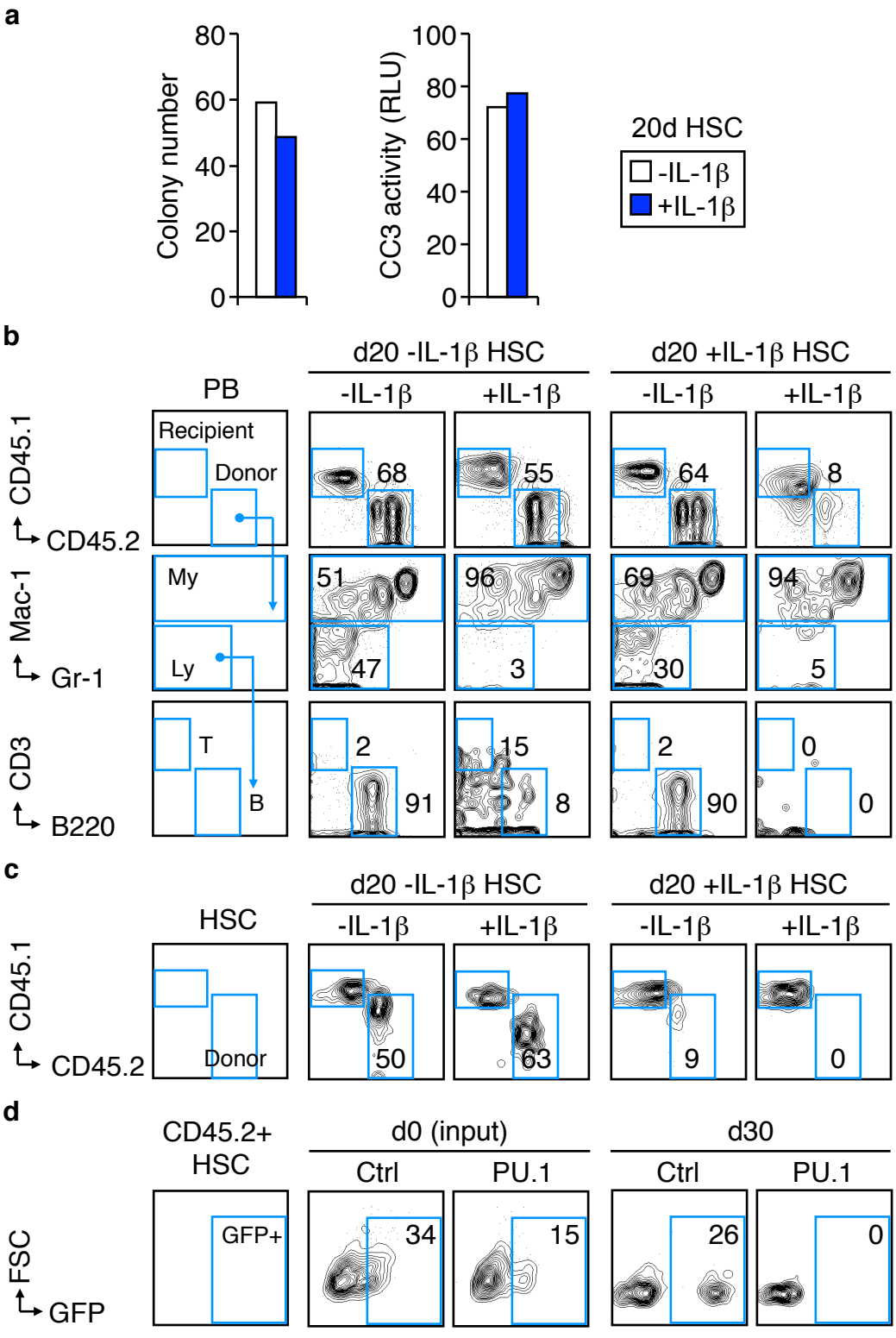

Fig. S7 (Pietras et al.)

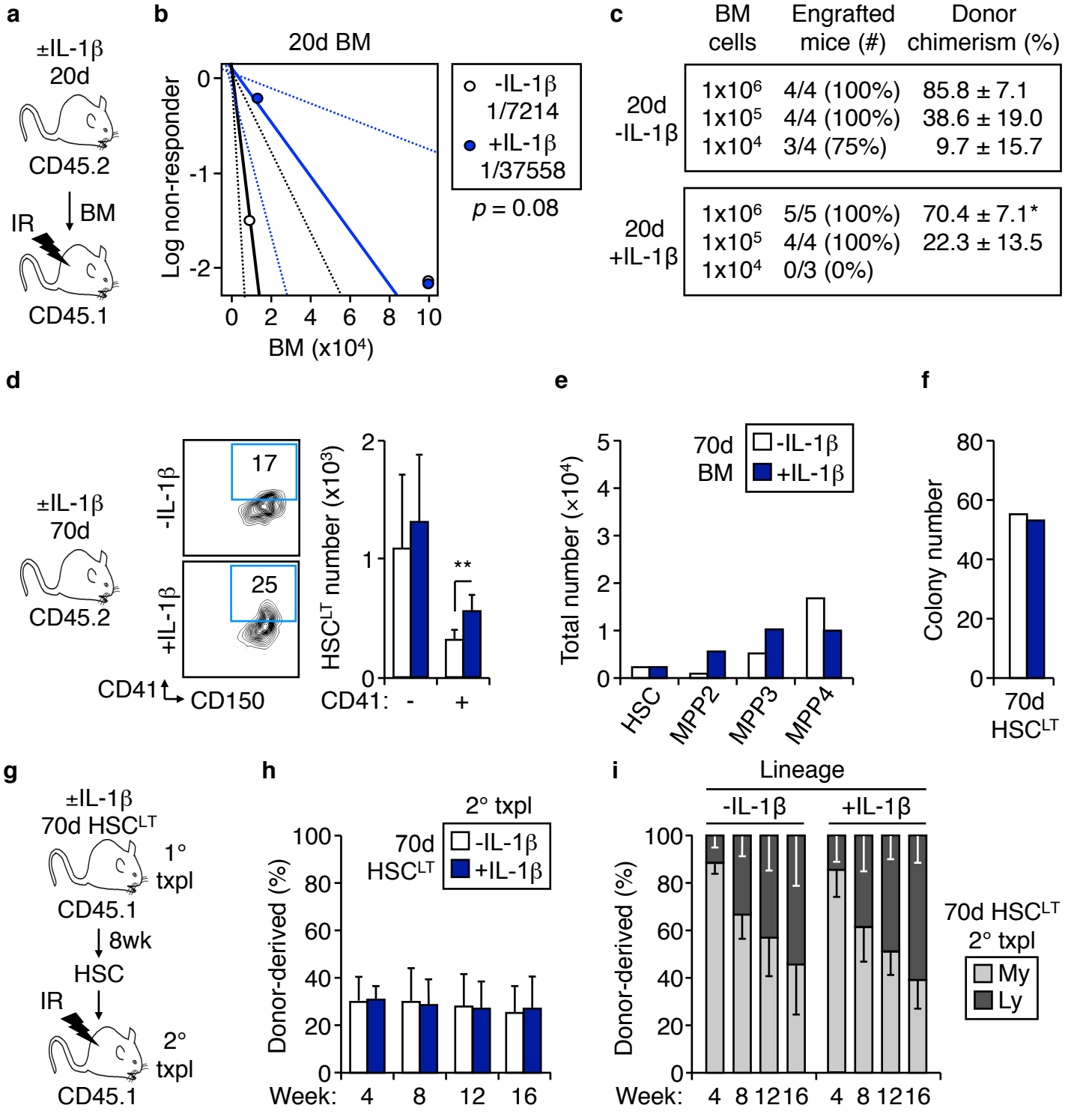

Fig. S8 (Pietras et al.)